Wind power in arctic conditions: The experience of Greenland

Branlard, Emmanuel

Publication date:
2010

Document Version
Publisher's PDF, also known as Version of record

Center for
ARKTISK TEKNOLOGI

Technical University of Denmark DTU

11427 - Arctic Technologies

Wind power in arctic conditions:
The experience of Greenland

Emmanuel Branlard

December 2010

Risø DTU
National Laboratory for Sustainable Energy

Center for
ARKTISK TEKNOLOGI

Contents

Introduction

The motivations for implementing wind energy in cold climates are rising and several small wind farm have already being installed in the subarctic areas. Among these motivations is the fact that most favorable and conventional sites have already been exploited and the need to extend the wind integration imply expending to more complex sites. The good availibility of wind in many world locations, is in favor of the use of wind for supplying energy to remote locations. A wide market potential is thus expected for wind energy projects in cold areas, in countries like Sweden, Finland, Norway, Iceland, China, Canada and mountainous areas of South America and Europe. It has been estimated[62] that about 20 per cent of the installed wind power within the European Union, which can be 8.000 MW by the year 2010, is going to be realized at sites were icing has to be taken into account in order to use the existing wind-energy potential The IEC-61400 standards recommends to take ice loads into account but a special load case is not given yet. However, experiences of wind turbines in cold climates show that heavy ice loads are not negligible and the case of Greenland is certainly the most extreme case of it.

In this report, the field work realized in Greenland will be described in a first part. In a second part, the description of the climate and topography of Greenland will follow, in order to get a better understanding of the conditions that wind turbines should withstand in this area. Following this description, the analysis of what these conditions imply as challenges for wind energy will be described. In a third part, solutions and recommendations to these challenges are presented in a general way. Eventually, in a fourth part, applications of wind energy in cold climate and most particularly Greenland are briefly presented. One of them being the need for TELE Greenland, the main telecommunication and postal provider in Greenland, to reduce their cost in providing energy to remote telecommunication towers. This report does no intend to provide a solution for this problem, but rather give the required background needed before investigating this question. Indeed, absolutely no knowledge about the field of icing, extreme climates, and vertical axis wind turbine was provided by the wind energy master at DTU. This project was such a great opportunity to feel this gap of knowledge for it to be hopefully applied for more practical purposes, like providing electricity to telecommunication towers.

Part I

Field work related to existing wind power in Greenland

Stay in Greenland

As part of the Arctic Technologies course(11427) at DTU, a three week trip to Greenland was organized from the 1^{st} to the 19^{th} of August. Supervised by Kasper Jakobsen a team of 9 people working or studying in the field of wind energy traveled around the area of Sisimiut $[66°55'57N\ ;\ 53°39'59W]$ to perform maintenance of wind masts and wind turbines. This field work took place in the villages of Assaqutaq, Sarfannguaq and Itilleq. A map of the area of Sisimiut with the different villages and the topography of the region is shown on Fig. 1. The different activities performed during this trip will be briefly described in the following chapters.

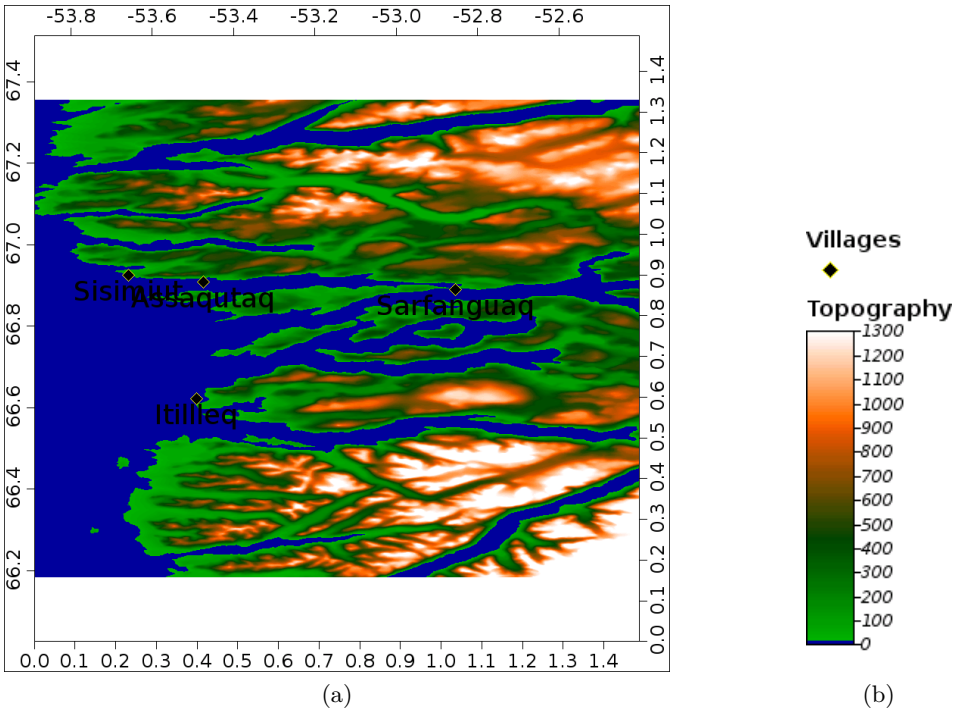

(a) (b)

Figure 1: Topographical map of the villages visited in longitude and latitude coordinates. (see Sect. 4.2 for details of the realization of this map with SAGA)

Chapter 1

Assaqutaq

1.1 Context

The village of Assaqutaq, located [66°54′54N ; 53°28′52W], is now an abandoned village on an small island with facilities that are mainly used for summer schools. Two houses and a church are still in well preserved as it can be seen on Fig. 1.1. In order to reduce the use of the diesel generator, solar panels, solar tubes and two wind turbines have been mounted around the formerly occupied house. Nevertheless, this system had never been tested yet at our arrival on the site due to the different voltages of the components involved. For more informations about this installation one can refer to the following references[64],[24] and [50]. Data from the solar panels and wind turbines have been interpreted for the short period(6 months) of data available by[63].

Figure 1.1: View of the best preserved houses of Assaqutaq village

1.2 Fieldwork

The fieldwork in Assaqutaq consisted in the following:

- Un-mounting and packing the meteorological mast present for further transport and installation in Sarfannquag
- Installing two SolData pyranometers one each side of the solar panels and ensure a clean cabling to the data logger. The angle of the the measurement devices has been set to be the same of the solar panel to ensure a reference reading of the irradiance measure.
- Mounting a met mast on top of the roof with a cup anemometer and vane, and cabling all along the roof top down to the data logger.
- Fixing of the electric system to enable battery charging.

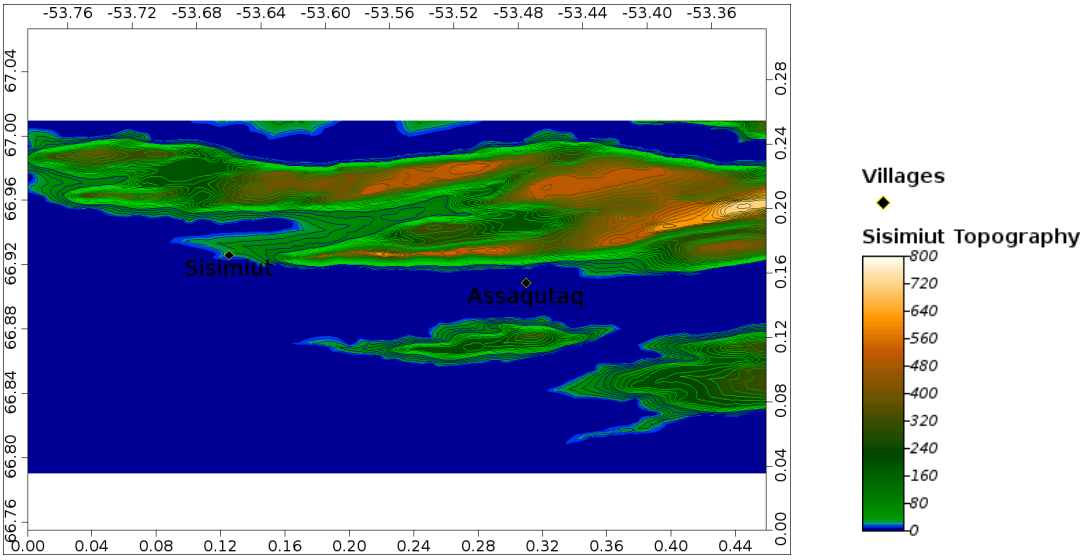

(a) (b)

Figure 1.2: Topography of Sisimiut area and Assaqutaq in longitude and latitude coordinates. (see Sect. 4.2 for details of the realization of this map with SAGA)

(a) (b)

Figure 1.3: Mounting of a small mast on a roof at Assaqutaq.

Chapter 2

Sarfannguaq

2.1 Context

The village of Sarfannguaq , located [66°53′50N ; 52°51′34W] has a population of around 100 people, and is located at the extremity of a fjord, but a small corridor of water links this fjord to a bigger one parallel to it. This special configuration makes this place subject to strong winds going from one fjord to the other. During summer 2009, a Proven6-300 wind turbine has been mounted at Sarfannquaq[34]. It is currently the largest wind turbine in Greenland, but had not produced any energy before the summer 2009 because the grid connection was not installed yet. Fortunalty, in parallel to our maintenance work during this summer 2010, this connection has been settled and the turbine produced energy for its first time the last day of our stay there.

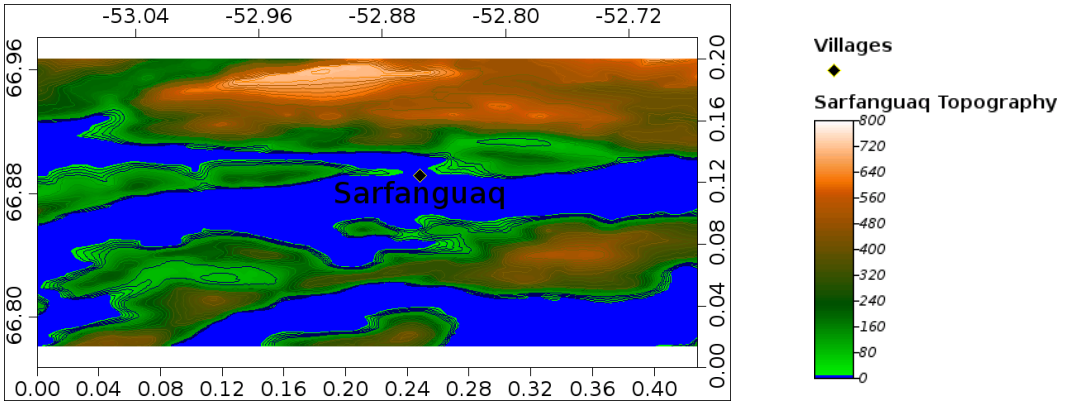

(a) (b)

Figure 2.1: Topography of Sarfannguaq in longitude and latitude coordinates. (see Sect. 4.2 for details of the realization of this map with SAGA)

2.2 Fieldwork

The field work in Sarfannguaq consisted in:

- Putting the old met mast to renew the sensors, add four booms and two cup anemometers for a total of 4 cup anemometers, renew the cables, and add an iPack to the data logger. The data logger had to be changed as it has been noticed that it was displaying erronous data.
- Performing maintenance on the wind turbine: the brakes pads were over used, the magnet was broken and one blade was damaged on the leading edge.
- Choosing a location for installing a new met mast. This location has to be within the high resolution topographical map, in a location where high wind speeds are expected, and with least disturbed flow on much sectors and particularly the main wind direction sectors.
- Installing the met mast from Assaqutaq at the chosen location and mounting several

sensors and solar panels on it. Unfortunalty, due to the failure of one of the data logger, no data+logger was available for this mast.

(a) (b)

Figure 2.2: Work on the wind turbine at Sarfannguaq. (a) The turbine being put down - (b) Work on the brake pads inside the nacelle

(a) (b)

Figure 2.3: Work on the old met. mast at Sarfannguaq. (a) Cabling and anemometers mounting - (b) Configuring the new data-logger with i-Pack

(a) (b)

Figure 2.4: Work on the new met. mast at Sarfannguaq. (a) Closeup on the instruments - (b) Sealing the box with silicon

(a) (b)

Figure 2.5: View of the two met. masts at Sarfannguaq at the end of the different tasks. (a) Old met. mast - (b) New met.mast

Chapter 3

Itilleq

3.1 Context

Itilleq , located [66°34′37N ; 53°29′49W], is a village of 120 inhabitants south of Sisimiut. A met. mast was installed one year before as the island is expected to have strong potential for wind energy. A project of installing a desalinization plant at Itilleq, partly powered with wind energy is currently studied. A project of using a wide roof surface for implementing solar panels is also in process.

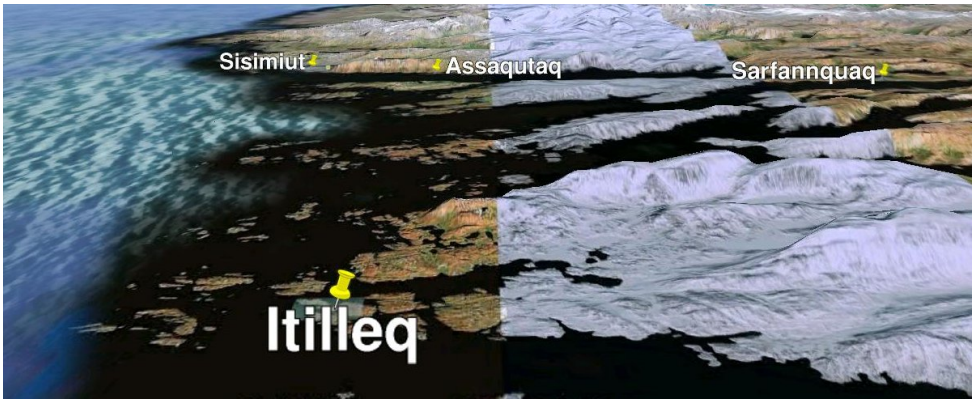

Figure 3.1: 3D view of the position of Itilleq with respect to the other visited village. Source: GoogleMap

3.2 Fieldwork

The field work performed in Itilleq consisted in:

- Putting down the met. mast to change the wind sensors.
- Moving the temperature sensor to the standard height of 2m
- Highering the new cup anemometer on a rod for its measure to be less disturbed by the mast
- Esatblishing a listing of all candidates roof that could host solar panel, reporting inclinaison, orientation and surface.

(a) (b)

Figure 3.2: Field work in Itilleq. (a) Partial view of the village - (b) The newly instrumented met. mast

Part II

Arctic resources and their challenges

Chapter 4

Greenland ressources

Motivations

Study of a challenging site In order to study the wind energy potential in Greenland it is important to understand the climates and landscapes that can be found in such a vast land. Indeed unlike most European countries, Greenland has only been starting to be considered as a potential place for wind energy since less than ten years. The experimental knowledge and data required for wind energy study is not here yet, and is progressively introduced with more detailed topographical maps, more wind masts and several small wind turbines being tested by DTU. Moreover, the conditions of Greenland makes really challenging the implementation of wind energy, and research is only at its early stage in the domain of icing and complex terrain for wind energy. This makes these early analysis challenging especially in the little amount of time provided for the project and the limited resources that a student can be given access to.

Wind turbine sitting for wind turbine sitting, a good knowledge of the wind and topography is required at the location of interest. In the prospect of the project no specific location is chosen, so that no deep study can be performed. Nevertheless, an overview of the resources of Greenland on a large scale is presented here, so that the method for data analysis are settled and could be applied in a smaller scale for wind turbine sitting.

4.1 Wind climate

4.1.1 Wind data available

DTU students from the wind energy master have a restricted access to the website *www.winddata.com*[25] and unfortunately no data has been retrieved from this website. In order to obtain long term data over several locations, the danish meteorological website[15] has been consulted as it offers archives data for Greeland under image format. The website contains 10 years of data for 10 different locations in Greenland corresponding to the main airports or heliports. Data were retrieved using several scripts specially implemented for this project, the source code being provided in Sect. A.1 of this report. The image data were requested with a script shell using the *wget* command, and then each image was interpreted with a *Matlab* script that reads the axis boundaries and detects the different curves of temperature, wind speed, pressure and precipitations. The data obtained are 6 hours averaged data at 10m height for the wind speed and 2m height for the temperature, which corresponds to the meteorological standards. Of course, these data should be interpreted carefully as they rely on the precision of the image reading algorithm implemented. The availability of the data is not optimal and the averaging period is too high for wind energy applications. Nevertheless, this was used to have an oversight of the mean wind speed found at several locations in Greenland. Main results will be presented in this report, but a more detailed view of the data can be found in the enclosed report performed within this project by the same author[10]. Few wind data analyzed by Risøin the 90's have been used to compare the consistency of the data and have more wind stations available. The

original idea was to get and insight of the wind atlas of Greenland from these measurement stations. Unfortunatly, this was rather optimistic given the size of the territory, the complexity of the landscape and thus complexity of the climate.

4.1.2 Wind ressource

The wind data analyzed from the DMI web site[10] and from RisøWASP climate TAB files are presented on Tab. 4.1. The different location of the mast are described and can also be seen on Fig. 4.4 on a figure realized with the free Geographical Information System(GIS) software SAGA and data from the Natioanl Snow and Ice Data Center (NSIDC)[43]. The mean wind speed at the observed location are rather low which was rather expected for locations in Greenland of low altitudes.

Table 4.1: Coordinates and height of masts, mean wind speed $\overline{U}$, Weibull distribution parameters A and k, 50 year extreme U_{50}, main wind direction θ_{main} and corresponding wind rose fraction p

City	Src	Long	Lat	H[m]	$\overline{U}$	A	k	U_{50}[m/s]	θ_{main} [°]	p
Aasiaat	DMI	-52d47'	68d43'	10	4.54	5.12	1.79	27.50	180	0.11
Ilulissat	DMI	-51d04'	69d14'	10	4.64	5.16	1.53	28.48	90	0.18
Ilulissat	Risø	-51d04'	69d14'	10	2.99	3.34	1.49	-	90	0.19
Ittoqqortoormiit	DMI	-21d57'	70d29'	10	4.22	4.11	0.94	92.30	30	0.20
Ittoqqortoormiit	Risø	-21d57'	70d29'	10	4.01	3.97	0.98	-	30	0.23
Kangerlussuaq	DMI	-50d42'	67d01'	10	4.06	4.57	2.50	20.22	60	0.43
Maniitsoq	Risø	-52d52'	65d24;	10	3.63	4.01	1.39	-	90	0.17
Nanortalik	DMI	-45d13'	60d08'	10	4.85	4.70	0.91	52.57	330	0.12
Nanortalik	Risø	-45d13'	60d08'	10	6.04	6.72	1.54	-	60	0.19
Narsaq	Risø	-45d58'	60d54'	10	3.58	3.78	1.14	-	90	0.12
Nuuk	DMI	-51d45'	64d10'	10	6.48	7.31	1.73	37.61	180	0.17
Nuuk	Risø	-51d45'	64d10'	10	6.79	7.62	1.76	-	180	0.16
Paamiut	DMI	-49d40'	62d00'	10	4.04	4.37	1.35	24.54	330	0.27
Paamiut	Risø	-49d40'	62d00'	10	4.46	4.85	1.30	-	330	0.20
Qaanaq	DMI	-69d23	77d29'	10	2.46	2.45	0.99	42.15	120	0.12
Qaqortoq	Risø	-46d03'	60d43'	10	4.95	5.21	1.14	-	60	0.15
Qasigiannguit	Risø	-51d10'	68d49'	10	3.26	3.53	1.25	-	30	0.21
Qeqertarsuaq	Risø	-53d31'	69d14'	10	3.90	4.27	1.35	-	90	0.29
Sisimiut	DMI	-53d43'	66d57'	10	4.00	4.39	1.39	28.80	90	0.20
Sisimiut	Risø	-53d43'	66d57'	10	3.66	3.99	1.30	-	60	0.17
Tasiilaq	DMI	-37d37'	65d36'	10	2.66	2.64	0.97	85.23	270	0.12
Upernavik	DMI	-56d08'	72d47'	10	4.30	4.77	1.48	43.71	90	0.15
Upernavik	Risø	-56d08'	72d47'	10	3.48	3.69	1.17	-	90	0.16
Uummannaq	Risø	-52d07'	70d40'	10	4.02	4.41	1.36	-	150	0.34

It was not possible to achieve a map of the wind ressources of Greenland from these data so external data from internet will be displayed here. The company *3*tier[2] offers world wind map at 80m height with a 5km resolution grid as seen onFig. 4.1. A zoom and rescaling of this world map allow of better view on the wind ressources of Greenland(see Fig. 4.2). High wind speed run on the high elevated ice cap, but this is of course not the locations of interest for implementing wind energy.

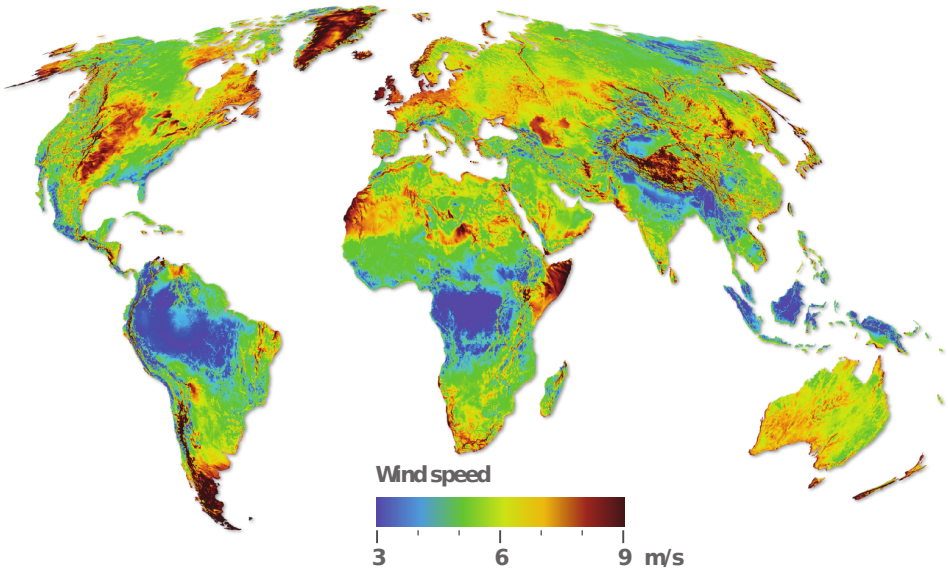

Figure 4.1: World wind map at 80m with a 5km resolution[2]

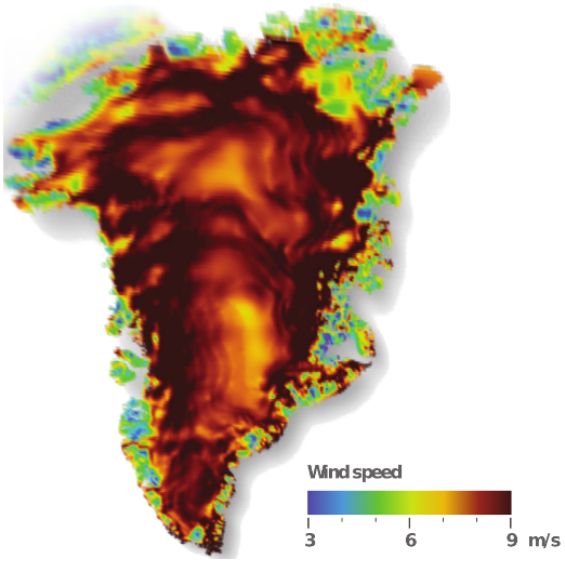

Figure 4.2: Wind map of greenland from Fig. 4.1[2]

4.2 Topography

4.2.1 Retrieving the data

For the study of the topography, data from the Natioanl Snow and Ice Data Center (NSIDC)[43] and [44] were used. The NSIDC provided topographical data of 3" arc resolution on an ftp server. It should be noted that a better resolution should be required for wind energy assessment with CFD due to the high complexity of the terrain. The data from this server have labeling that corresponds to the longitude and lattitude over greenland. These are displayed on figure Fig. 4.3 together with the UTM zones. The vast area of Greenland and the fact that it is close to the pole imply that Greenland spreads on a wide longitudinal range from 12°W to 73°W. One file correspond to a grid of 1°N and 1°S. In total more than 700 files are required to describe Greenland.

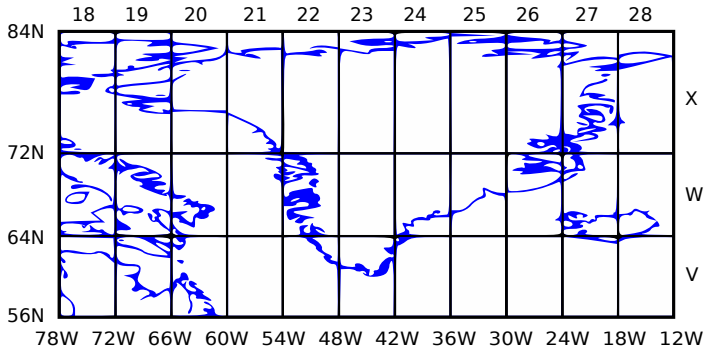

Figure 4.3: UTM zones over Greenland

These data were concatenated, into one main file representing the whole Greenland. The resulting file sized 2Go. To enable a decent manipulation of the file with the free Geographical Information System(GIS) software SAGA, the resolution of the data has been reduced.

4.2.2 Coordinates conversion

The coordinates of the data were provided in longitude and latitude and had to be converted to a stereographic projection coordinate system for a more conventional view of Greenland. The view of Greenland in longitude and lattitude coordinates looks indeed different. To obtain Fig. 4.4 the coordinates of the meteorological stations had also to be converted. This conversion was done with the free command line tool proj4. The following command was performing the conversion:

```
proj +proj=stere +lat_0=90 +lon_0=-45 StationsCoordinatesLongLat.txt
```

With the file *StationsCoordinatesLongLat.txt* containing the longitude and lattitude coordinates in the following format:

```
1  -69d23   77d29'   16      Qaanaq
2  -56d08'  72d47'   126     Upernavik
3  -51d04'  69d14'   29      Ilulissat
4  -52d47'  68d43'   23      Aasiaat
5  ...  ...  ...
```

4.2.3 Manipulation with SAGA-GIS software

The following figure was obtained with the use of SAGA software: for the whole Greenland area:Fig. 4.4, and the figures previously shown for the area visited during our stay in Greenland Fig. 1, with close up on the area of Sarfanguaq and Sisimiut respectively on Fig. 2.1 and Fig. 1.2

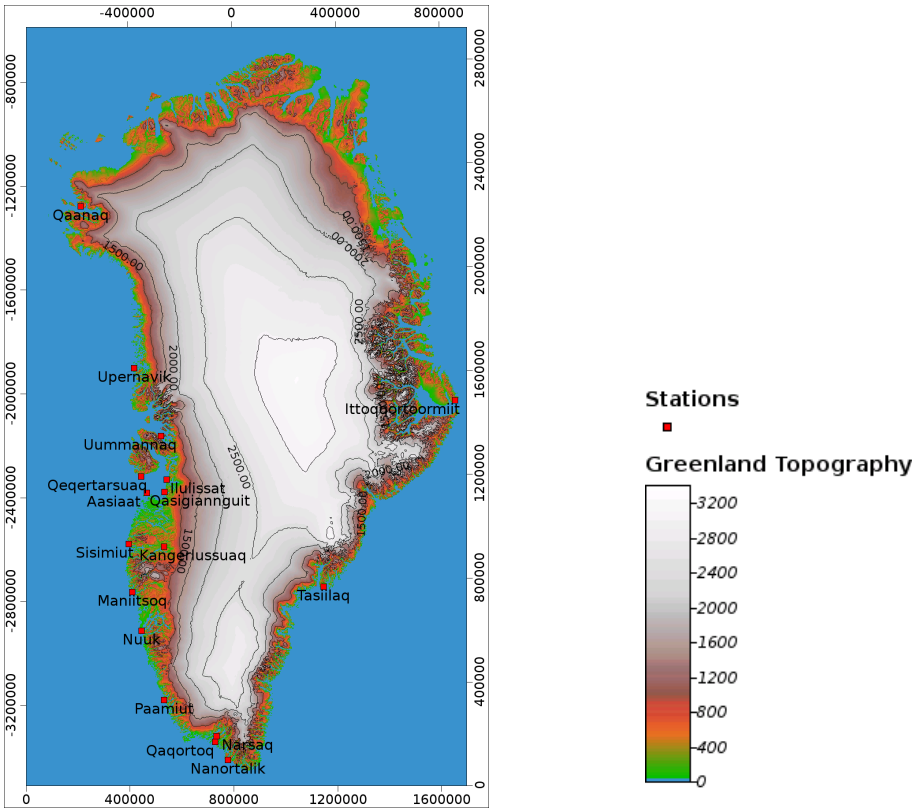

(a) (b)

Figure 4.4: Greenland elevation map. (a) Meteorological stations available - (b) Elevation map only. These map were realized with SAGA-GIS, with topographical data from NSIDC[43]

4.3 Temperature

4.3.1 Data used

A brief overview of the temperature is shown here. Data from the Intergovernmental Panel on Climate Change(IPCC) website [29] were used for world temperature map. In the following mean values for the period 1961 to 1990 are shown, first for the entire world and with average over the seasons, and then only for Greenland with the monthly evolution. Data such as the number of day of frost ground can also be retrieved on this website. Data were downloaded in the NetCDF format, then imported in HDFView to be exported in table form. Then SAGA could have been used to read this grid as a table, but the choice of the programming language R has been made, to automatize the process of data manipulation. R source codes can be found in Sect. A.2. **??** shows the mean temperature over all seasons for the year 1961 to 1991 whereas Fig. 4.6 shows the seasonal evolution of the temperature for this period.

4.3.2 Mean temperature without seasonal variations

Figure 4.5 shows the mean the temperature for the period 1961 to 1990 for the whole globe and for Greenland.

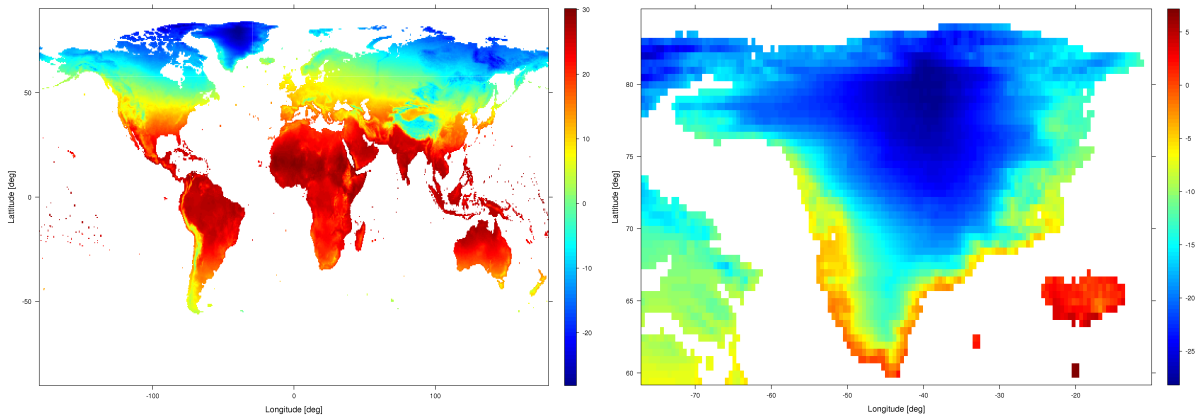

(a) (b)

Figure 4.5: Mean temperature during the years 1961 to 1990. (a) World map - (b) Greenland map. Figure realized with the data from the IPCC[29]

4.3.3 Mean temperature of Greenland with seasonal variations

Figure 4.6 shows the seasonal evolution of the temperature for the period 1961 to 1990 in Greenland. This gives an overview of the temperature expected at a given location. Given the large amount of data found on the IPCC website, ground frost frequency, precipitation, minimum and maximum temperature, etc., a lot of results could be provided. Also, the yearly variations of these parameters could be studied but his would go out of the scope of this project.

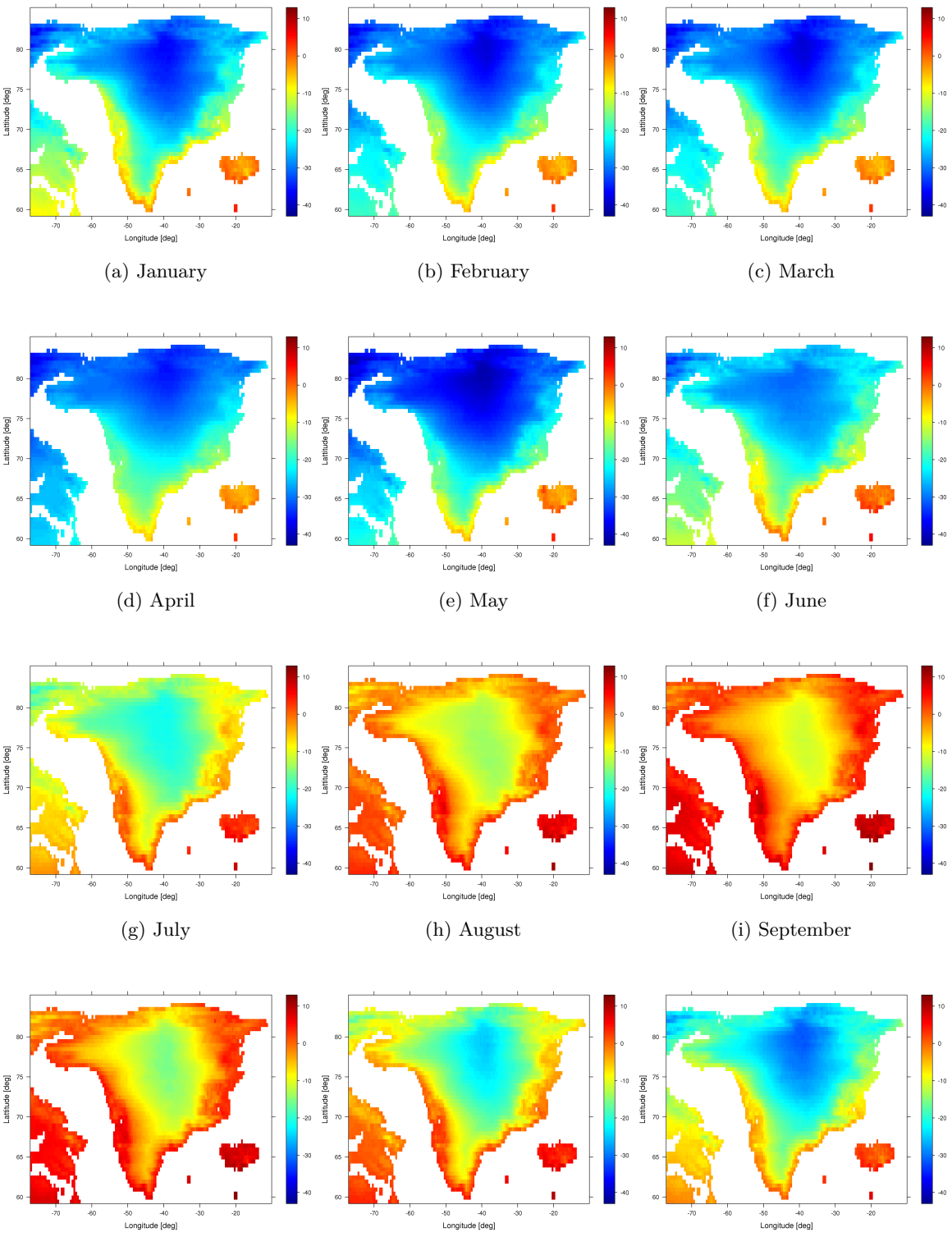

(a) January (b) February (c) March

(d) April (e) May (f) June

(g) July (h) August (i) September

(j) October (k) November (l) December

Figure 4.6: Mean evolution of monthly temperature during the year - Mean values from 1961 to 1990

Chapter 5

Understanding the challenges of cold and mountainous site for wind energy

5.1 Greenland, a cold climate site

Cold climate site From the Germanischer Lloyd Wind standards a low temperature site is a site with more than 9 days presenting at least one hourly temperature of less than -20°or with a yearly mean temperature of less than 0°. The IEA Wind task 19[28] defines a cold climate more simply as a site where either icing events or low temperatures that are outside operating range occur. A cold climate can present any of this characteristics:

- Air temperature below zero degrees for long periods during the year
- Clouding in proximity of the ground surface (see Fig. 5.1)
- High water content from atmosphere

Such conditions are likely to be associated with extreme conditions, complex terrain and site elevation typically found in mountainous regions, sub arctic and arctic regions and some offshore locations. Greenland matches all of the above criteria.

Figure 5.1: Clouding close to the ground surface observed during th e summer 2010 in Greenland. Combined with low temperature, in-cloud icing is likely to happen in such conditions

Qualification of Greenland as a wind energy site Greenland enters clearly in the category of none-conventional sites for wind energy implementation. A conventional site would be a site located in a wide and windy area with temperate climate, good knowledge of meteorological data and a favorable landscape with few obstacles. On the opposite, a non conventional site would typically include hostile climates. Depending on the location, non conventional sites can be separated into hot climate and cold climate sites.

5.2 Challenges from the landscape in a mountainous area

5.2.1 Orography

Orography is the study of the formation and relief of mountains. The first effect of the orography is to induce changes in the pressure fields of an existing flow. The windward side of a hill is blocking the flow with a well known speed up at the top of the hill. The flow is also forced in a lateral motion when going around a hill, or when canalized between two hills or cliffs(see Fig. 5.2). Orography has also an indirect effect due to the difference of absorption of the earth surface depending on land inclination and orientation. This is responsible for thermal induced flows typically illustrated with the day and night hillside wind patterns respectively blowing up-slope and down-slope in mountainous areas.

Figure 5.2: Landscape in Greenland. Fog going moving quickly from one fjord to the other, passing through a small channel delimited by two cliffs. On this figure also, the high complexity of the terrain can be seen.

5.2.2 Terrain complexity

The wind field is highly perturbated by the complexity of the landscape which creates flow separation and large-scale turbulent structures. The vertical wind profile can thus have many different shapes with even negative gradients occurring. The wind profile is also really likely to be wind-sector dependent due to surrounding obtacles, and this is contrary to conventional sites with rather flat terrain, where only one wind profile is assumed. An illustration of the high terrain complexity where the wind turbine is located at Sarfanquaq can be seen on (see Fig. 5.2).

5.2.3 Territorial uses

When studying the implementation of a wind turbine, several territorial factors will also have to be dealt with. In cold climate sites, it is likely to find few infrastructures (roads, electrical grid) and few population. This will raise logistical questions of site availability, dimensions of the wind turbine, and the distance from the grid which can add additional costs. In a more general way, one has also to avoid natural parks, military areas, historical and archaeological sites and marine routes in the case of offshore.

5.2.4 Effect of turbulence and wind shear

Turbulence implies more fatigue on the turbine, it can also imply an hysteresis effects around cut-in, rated, and cut-out wind speeds that will make the control and the grid connection/disconnection more difficult.

Wind shear will imply fluctuating loads and the rotor, and the variability of wind shear with temperature, stability of the atmosphere and wind sectors will imply more uncertainties on the wind speed determination and thus on the power production.

5.3 Influence of the climate on wind energy

5.3.1 Extreme events

Extreme events will imply increased loads and fatigue, damage and potential energy losses. Slight or moderate rain does not influence the performance of the WT but heavy rain can induce power losses up to 30% due to drop impacts. Hail will mostly imply damages on the blade leading edge with high wind speed impacts. Lightning can involve serious damages of the rotor blades and the electric components under a direct strike. Indirect impact would damage mostly components that are not protected against over voltage.

Extreme Temperature Materials and lubrifiant present in the wind turbine are designed to withstand a given range of temperature, outside of which increased maintenance may be required, accelerated loss of equipment life will occur and damage to equipment may result[8]. It should be remembered that material properties such as Young's and Poisson's modulus are temperature dependent. Two temperatures are defined by the manufacturer. The minimum ambient temperature below which operation is stopped, and the standstill temperature which is the temperature the turbine can withstand. Extreme temperatures would imply stresses on the material that would wear or tear them.

5.3.2 Influence of temperature and air pressure on power performance

Understanding the influence of temperature and air pressure is of prime importance either for the design of a new wind turbine, or for adapting an existing wind turbine to a cold climate location. Most of the time indeed, a wind turbine designed for conventional sites will produce less in a montainous area, and thus design compensations for this energy drop have to be found like increasing the rotor diameter, elevating the tower, changing the rated wind speed.. These strategy choices are delicate and should be compared versus each other to find the most economic way. Also, several cases of unexpected high power production of stall regulated wind turbines operating under low temperatures have been reported.

Definition of key paranmeters Air density ρ, dynamic viscosity μ, kinematic viscosity ν, and Mach number M are function of temperature and/or height according to the following relations:

$$\rho = \frac{p}{RT} \tag{5.1}$$

$$\mu = \sum a_i T^{i-1} \tag{5.2}$$

$$\nu = \frac{\mu}{\rho} = K\sqrt{\frac{\tau_0}{\rho}z} \tag{5.3}$$

$$M = \frac{U}{a} \quad \text{with e.g. } a_{\text{air}} = \sqrt{\gamma_{\text{air}} R_{\text{air}} T} \tag{5.4}$$

with the temperature T in Kelvin. For the air the values $\gamma = 1.4$ and $R = 287$ can be used.

The relevant dimensionless numbers for atmospheric flows are the Reynolds, Richardson and Lewis numbers described in Tab. 5.1

Table 5.1: Dimensionless numbers relevant for wind energy in cold climate

Name	Definition	Influences
Reynolds	$Re = \frac{\rho U c}{\mu}$	Aerodynamic performances, wake, heat exchange process
Richardson	$Ri = \frac{2g\frac{dT}{dz}}{dT\left(\frac{dU}{dz}\right)^2}$	Air stratification, shear stresses and wind profile
Reynolds	$Le = \frac{k}{\rho c_p D_{\text{air/vapour}}}$	Evaporative mass transfer

The temperature and pressure will be smaller than normal in mountainous areas. In arctic or sub-arctic plains only the temperature will be smaller. It will be expected in general to have ρ, Re, power and loads higher in sub-arctic plains, and lower in mountainous areas.

Effect of Re Historically, airfoils used in wind energy are often used at Re that are lower than the one they were designed for. As Re decreases, the maximum lift coefficient decreases and stalls earlier. At low Re, the C_l is even more deteriorated with changes of the slope $dC_l/d\alpha$ due to the apparition and separation of laminar bubbles. The Re effect will no be critical for large turbines but expected to be more important for smaller wind turbines. This effect is also reduce when the airfoil data are measured in wind tunnels of low turbulence intensity, because higher turbulence will postpone the stall transition. Typical Reynolds number found for wind energy are displayed on Tab. 5.2. The reynolds number have been estimated using the rotational speed and the chord length: $Re \approx \frac{\rho \omega r c}{\mu}$.

Table 5.2: Typical Reynolds number of several wind turbine under standard conditions and for nominal speed

Section	0.6 MW	1.0 MW	1.3 MW	2.3 MW
Root	1.7 10^6	2.2 10^6	2.5 10^6	3.9 10^6
Mid	2.7 10^6	3.3 10^6	4f.2 10^6	6.1 10^6
Tip	1.7 10^6	1.7 10^6	3.4 10^6	4.0 10^6

Effect of air density The effect of air density should be studied carefully, by performing for instance different BEM calculations. A decrease of air density will of course result in a power drop that has to be compensated for with a new design. Air density effects are easier to investigate than Re effects.

Mach number and incompressibility The hypothesis of incompressibility is often used for Mach number below 0.3. Evaluation of Mach numbers according to Eq. (5.4) is done for two wind turbines of different size and rotational velocity the results being presented on Tab. 5.3.

Table 5.3: Evaluation of Mach numbers for two typical wind turbines at different operating conditions and blade span location r/R

Wind speed			5m/s				25m/s			
Temperature			-25°		25°		-25°		25°	
R [m]	Ω [rpm]	r/R	25%	100%	25%	100%	25%	100%	25%	100%
41	27		0.09	0.37	0.08	0.34	0.12	0.38	0.11	0.34
2	60		0.02	0.04	0.02	0.04	0.08	0.09	0.07	0.08

5.4 The importance of resource estimation

Measurement is more difficult and less accurate in complex terrain due to the high turbulence and the presence of vertical flow angles. The mast and measuring equipment is also undergoing strong loads(gusts and ice) which will reduce the accuracy of the results and will sometime make it difficult to keep the mast erected. The interpreation of the measures should be done carefully, as it is hard to assume that the wind statistics at the measured site is characteristic of the wind at the wind farm site. If the wind turbine and the masts are placed on a hill, one can expect differences of wind speed of 1 to 5% depending on the relative positions of the mast and the turbines. In a mountainous area where more flow recirculatin are found, one can see differences up to 40%. Despite the positive speed up effect over a hill, there are indeed a lot of turbulent and recirculating zones that makes the wind highly variable even locally. For this reason the use of numerical or physical models should be combined to the field measurement to obtain an accurate wind ressource estimation and thus an accurate power production assessment.

Ice accretion on wind turbines is difficult to predict from the site measurements which are stationary and thus difficult to correlate with the resuls on the rotating structure.

Chapter 6

The nature of icing

Icing on wind turbine blades will influence the aeroelasticity of the turbine and raises the safety question of ice falls and ice throws. A small description of the icing phenomena, and mostly on ice accretion on objects is done in this section together with the influence of icing for wind energy. This will allow a better understanding of the intensity of the process to find way to prevent icing events and how to detect icing events from measurements.

6.1 Generalities

The physical mechanisms associated with ice accretion are complex because they involve meteorological processes(liquid vapor, supercooled droplets), mechanical processes(motion of the structures involved), and thermodynamic mechanisms(energy balance). The main parameters for icing are by order of importance:

- The liquid water content of air (LWC)
- The air temperature (T)
- The droplet size (MVD)
- The Wind speed
- The atmospheric pressure

The different kind of icing Icing can occur in different situations and takes different forms:

- In-cloud icing: occurs if the height of cloud base is less than the site elevation and the temperature at the site is below zero
- Freezing precipitations: occurs when it is raining and wet-bulb temperatures lies below zero
- Frost: occurs when the surface temperature drops below the frost point temperature
- Wet snow and sleet: occurs when a positive heat flux from the environment melts the surface of dry snow flakes.

Icing conditions are of different intensities at different locations of the globes and also different altitudes. In Europe, a typical light icing site would be located at 1000 m above sea level (a.s.l.), and an heavy icing at 2000 m.a.s.l.

Ice accretion and sources of ice Ice can be formed from water droplets, water vapor and from snowflakes, creating different kind of ice accretion:

- Glaze and rime are formed from water droplets from clouds or fog
- Frost is formed from water vapor
- Wet snow is formed from snowflakes

For wind turbines sites, the conditions of icing could be met in the presence of clouds, fog, snow, freezing rain, and for offshore locations sea sprays.

6.2 From water droplets to glaze and rime

Conditions Glaze and rime will occur if the surface of the object has a temperature beneath 0°and if it is impacted with water droplets. If the temperature of the droplet is below the freezing points, they are in an unstable state and are qualified as supercooled. They will freeze almost immediately by contact. They are often found in stratiform(likely to produce rime) and cumulus(likely to produce glaze) clouds. To experimentally perform supercooled water, the water should be cooled at a really fast rate of the order of $10^6 K/s$. The process is governed with the characteristics of the air flow which caries the water droplets and the colliding structure geometry and functional characteristics. Figure 6.1 illustrates the dependency in temperature and wind speed for the different of icing from droplets.

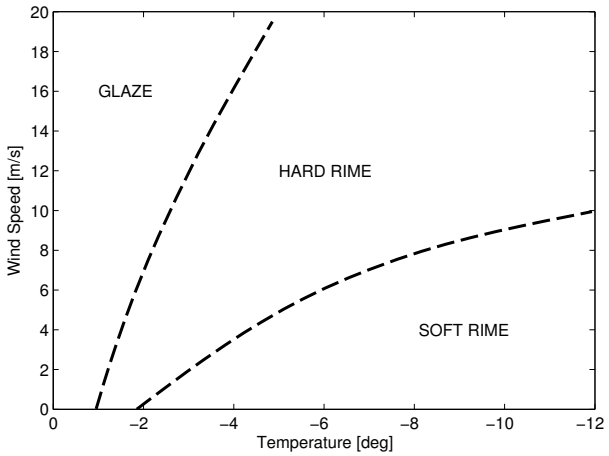

Figure 6.1: Distinction of the different icing from supercooled droplets with wind speed and temperature. The distinction with data from measurements

The freezing process During a first stage a part of the droplet freezes rapidly. To do so, it releases the latent heat of fusion which will raise the temperature of the remaining water to 0°. In a second phase, the droplet releases heat to its environment by convection evaporation and conduction , and thus freezes progressively. This second phase has a characteristic time τ with typical values around 10^{-3}s.

Ice accretion types Depending on the time duration Δt between two droplets strikes at a same location, and depending on the freezing process characteristic time *tau*, different type of ice will be formed:

- $\tau << \Delta t$: soft rime with dry growth
- $\tau < \Delta t$: hard rime OR glaze in the case of freezing rain
- $\tau \geq \Delta t$: glaze with wet growth

When the surface temperature is below zero, it is said that the ice accretion occurs in dry-growth conditions, as opposite to wet-growth when the surface temperature is at 0°. Figure 6.2 illustrates the accretion of ice for glaze and rime.

Ice accretion rates Ice accretion rates increases approximately at constant rates with time in a rime icing conditions, whereas with increasing rates in glaze icing conditions. The mass of ice collected on a surface depend on the liquid water content in the air flow, the collision efficiency of the droplets, the wind speed, the area of the cross section of the structure, air temperature

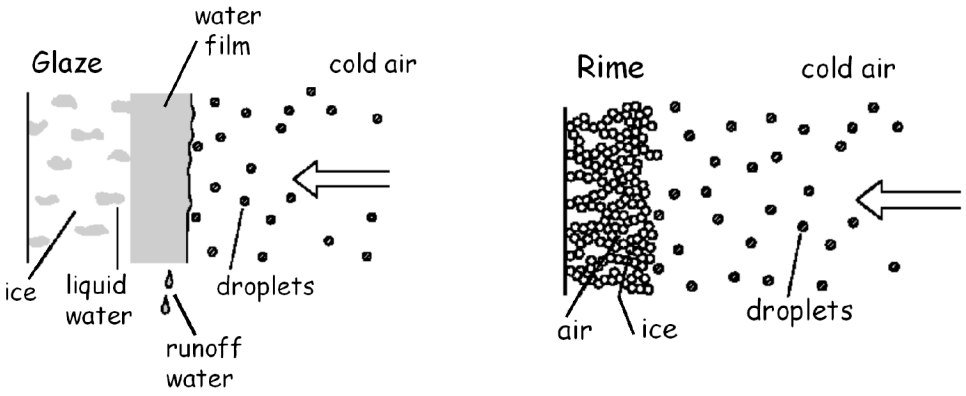

(a) (b)

Figure 6.2: Accretion of ice for supercooled droplets[8]. (a) Glaze - (b) Rime

and time. Poor amount of observations are available for this kind of icing which occurs mainly in clouds, and thus often in a different conditions than the meteorological stations as illustrated on Fig. 6.3. Freezing rain on the opposite is well observed because it happens due to a change in temperature sign close to the surface.

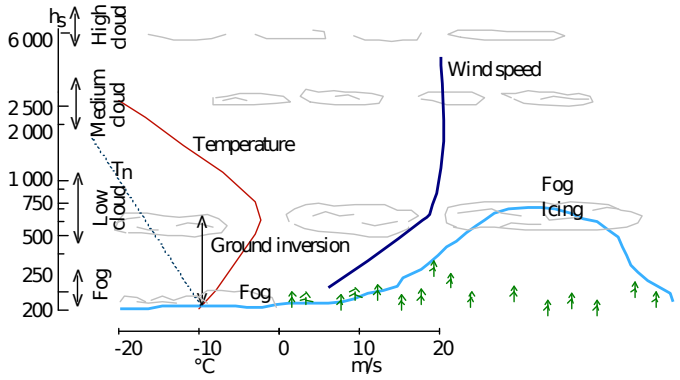

Figure 6.3: Illustration of in-cloud icing, and the difficulty to use meteorological station measurements[56]

6.3 Distinction of the different kind of icing

The classification of the different kind of ice is made difficult by the resemblance between them and also the fact that in our daily life, one word is often used for another when qualifying ice. A better knowledge of their characteristics and a view of the look of the different ice types will help their distinction. Table 6.1 references several of these characteristics, while Fig. 6.4 illustrates them. As mentioned above, icing conditions can be distinguished by the source but also by their density.

(a) Hard Rime (Photo Jean-Pierre Baubet)

(b) Soft Rime

(c) Glaze

(d) Frost (Photo Andrew Dunn)

Figure 6.4: Illustrations of the different type of ice

Table 6.1: Ice accretion types

	Hard Rime	**Soft Rime**	**Glaze**	**Frost**	**Wet snow**
Source	Droplets	Droplets	Droplets	Vapor	Snowflakes
Size [mm]	0-10	0-10	0-500		4-20
Density [kg/m^3]	600-900	100-600	900	<900	200-990
Air Temperature [°]	-2 to -10	-2 to -10	0 to -5	below 0	just above 0
Surface temperature [°]	Below 0	Below 0	0		
Conditions	supercooled droplets, in-clouds	supercooled droplets, in-clouds	supercooled droplets, rain or fog	high water vaport content	High liquid vapor content
Accretion	accretion against the air flow in the form of humps,fragments easily separates		Small accretion	Small accretion	get easily compact
Look	granular, white or translucent	white or opaque, milky and crystalline like sugar	transparent with glassy surface, bubble free, strong adhesion	translucent,cry spike-like or scale-like structures	granular, dense

Chapter 7

Icing and wind energy

7.1 Presentation

The focus of this section is the influence of icing on wind energy. The different aspects that icing affects can be listed as:

- The wt design: aerodynamics, loads, dynamics, control system, instrumentation, material
- The safety: Ice throws, noise, unbalance, resonance, over power, fatigue
- The economics: Energy production, design life time, site prognosis, wind measurement, wind turbine equipment

Among the different kind of icing described in the previous section, in-cloud icing is the most severe icing in wind turbine operational conditions. The effect of icing will lead to increased roughness of the blade during stand still and reduced power production during operation. Even over production can be noticed due to increased chord length of the blade. Several classes of icing can be defined for wind turbine sites:

1. No icing
2. Occasional icing: probability of icing of less than 1 day/year
3. Light icing: few days of icing, 1-7 days per year
4. Moderate icing: 8-14 icing days, monthly power loss less then 5% - occasional problems with control anemometers and public safety - not significant loss in annual power production;
5. Strong icing: several days of icing of blades, 15-30 icing days, power loss 5-15%
6. Heavy icing: icing of blades very typical during the winter period, number of icing days more than 30, power loss 15-25%.

7.2 Aerodynamics and ice accretion on wind turbines blades

7.2.1 Description

Ice accretion occurs prevalently on the leading edge(LE) of the rotor blade, with more and more ice collected at the stagnation point as the rotor turns. Due to the increasing air velocity along the radius, the ice accretion builds up more at the outer part of the blade with an approximately linear increase. With growing ice accretion the drag of the airfoil increases diminishing the power output of the turbine. Illustration of ice accretion can be found on Fig. 7.1.

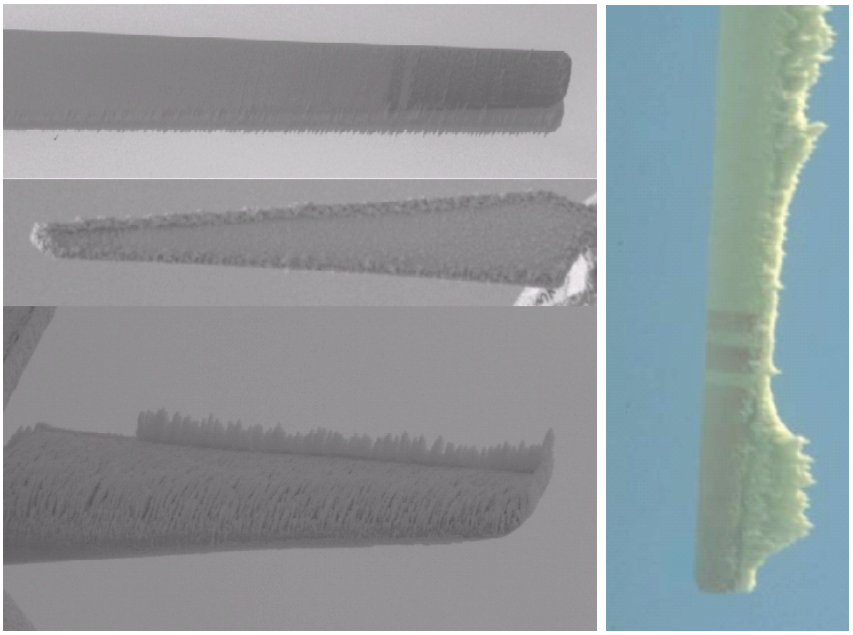

(a) (b)

Figure 7.1: Ice accretion. (a) Pitch regulated turbine operating, with LE accretion(top). Stall regulated turbine at low wind (middle) and iced trailing edge while parked (bottom).- (b) Rotor blade iced during idling [62]

7.2.2 The WECO project

The Wind energy production in cold climate(WECO) project[56] was carried out during the years 1996 to 1998. Several experiments were carried out with NACA 4415 with different ice accretion shapes and thicknesses. The main results are presented here, but more documentation can be found in [56]. The airfoil coefficients obtained experimentally can be found on Fig. 7.2. An estimate on the power reduction from these different kind of icing can be found on Fig. 7.3. Where it can be seen that the rated power either reached later or never reached, with a production largly reduced. The accretion of ice with time has also been studied experimentally and

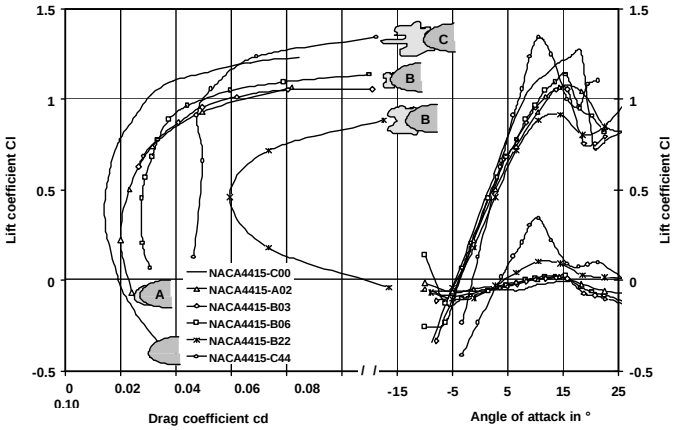

Figure 7.2: Aerodynamic coefficients obtained from wind tunnel measurement with the NACA4415 airfoil and several ice accretion shapes[56]

numerically, with the results seen on Fig. 7.4 Eventually the dynamic behavior of the profiles has been studied, and an example of results is shown on Fig. 7.5. No significant influence of

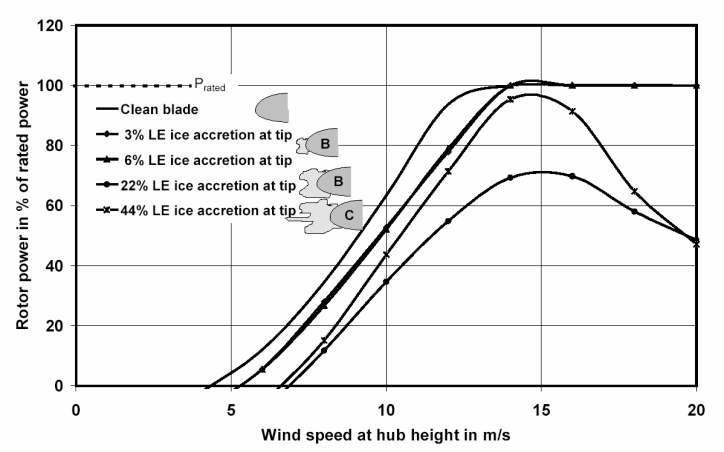

Figure 7.3: Power curve simulation for a pitch regulated turbine under three ice accretion cases[53]

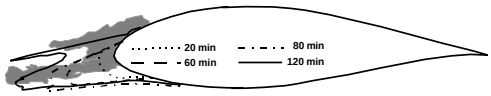

Figure 7.4: Ice accretion with time[56]

icing on dynamic stall were found, but the amplitudes of oscillations were lower.

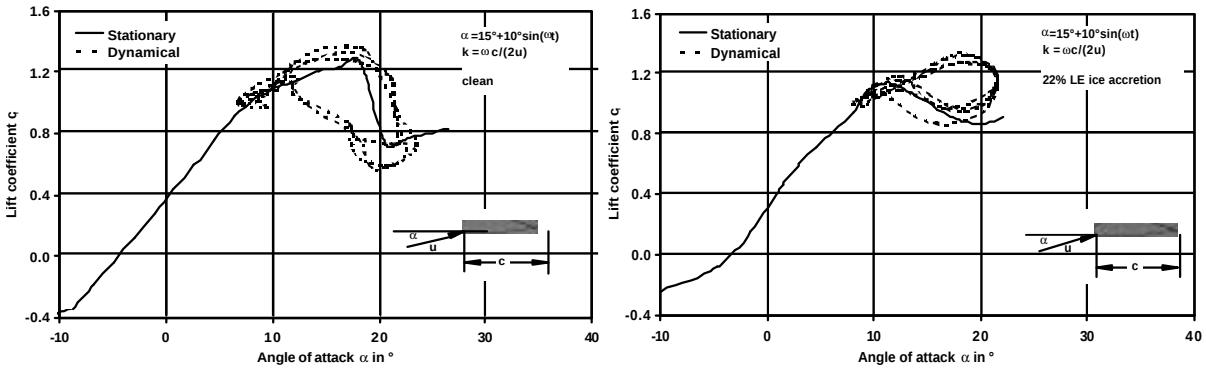

(a) (b)

Figure 7.5: Dynamic stall. (a) Clean airfoil - (b) Iced airfoil (22% type B)

7.2.3 From experiments and simulation to extrapolation

Currently several results can be found in the literature obtained with experimental methods(e.g. [56]). Unfortunately to predict the performance of the wind turbine under icing conditions, one needs data at several angles of attack, for different airfoil shapes and for a wide range of chord and thus Reynolds number. Experimental results from a different airfoil under icing can be used to extrapolate the coefficients of the known clean airfoil. The description of the extrapolation method is done in [56], but the main idea and equation is shown on Fig. 7.6. The extrapolation is based on the affine relation between the interval of the zero lift and the maximum lift angle of attacks. This affine relation is determined from the known $C_{l,NACA}$ of the reference experiment with clean airfoil(subscript NACA) and the known $C_{l,NP}$ of the New Profile where no ice experiments are available(subscript NP). Once the relation is found, one can determined the extrapolated coefficients for the new profile under icing from the reference values of the experiment fro the NACA profile. In case the airfoil coefficients used for extrapolation

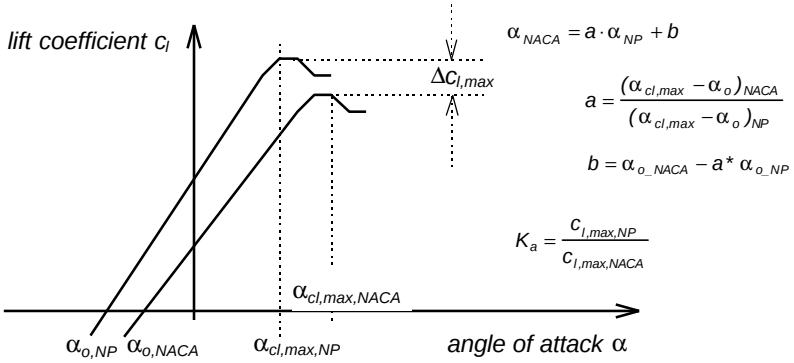

Figure 7.6

where normalized with the standard chord size a correction should be applied to include the length of the ice accretion. If this is not done, one could obtain lift coefficient that increases with icing which is not expected.

Numerical prediction is of great help but is not efficient enough currently, and glaze, which is the most commonly seen on wind turbine, is difficult to model. Despite the large amount of research results from the aeronautic industry, a little knowledge can be derived from this field as the icing exposure time are way larger for wind turbines. The three most famous and specific tools used to perform ice accretion prediction are: Lewice[33], Turbice[36, 18] and Antice[6].

7.3 Action of icing on the wind turbine structure

7.3.1 Ice accretion

As few meteorological data are available concerning liquid water content and droplet size, empirical relations are often used to estimate the ice accretion. In ISO 12494 [1], the accreted mass is assessed as:

$$m = 0.11 \cdot U \cdot \Delta t_h \cdot L \text{ [kg/m]} \tag{7.1}$$

with U the wind speed in m/s, Δt_h the duration time spent in-cloud time in hour and W the length of the object. Another empirical formulation used, is the one presented in BOREAS III conference[61, 57, 8] that give the intensity of rime accretion in kg/m^2/h as follow:

$$M = 0.045 \cdot a \cdot U \cdot \Delta t_h \tag{7.2}$$

with a the relative amout of cloud in %. In the two empirical formula above the ice mass changes with height z because the wind speed and the length of the object do so. The repartition of ice along the height of the tower for different tower elements with respect to their self weight is displayed on Fig. 7.7a. A increase of 1.4% of the tower mass is in overall expected which would decrease the tower eigenfrequencies. For the rotor blades, the blade thickness together with the relative wind will play a role on the accreted ice mass. This is illustrated on Fig. 7.7b.

7.3.2 Icing and fatigue

The question of whether ice increases fatigue loads seems questionable because arguments for increase and decrease of fatigue loads can be listed[56]. The reasons for which ice would increase fatigue loads would be:

- Additional masses increasing the gravity loads

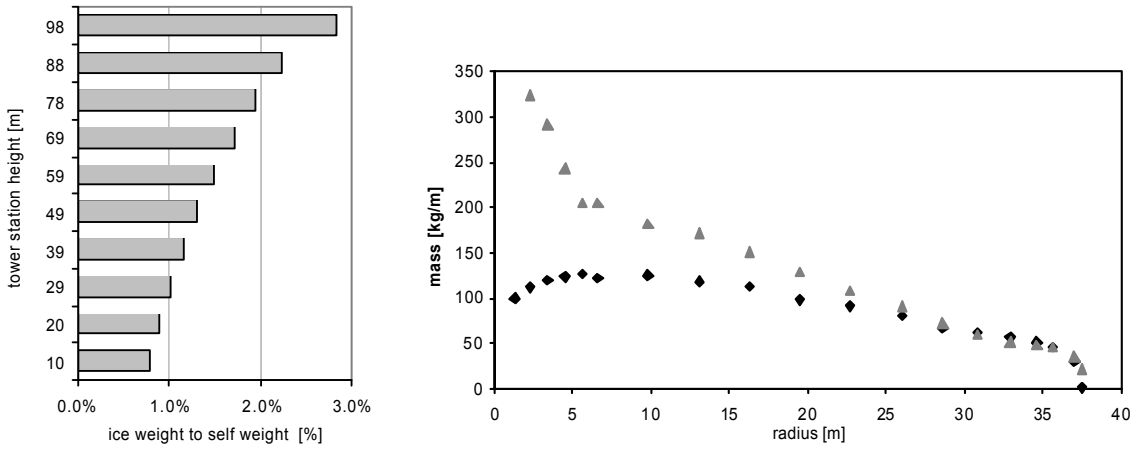

(a) (b)

Figure 7.7: Distribution of ice on wind turbine components[23]. (a) Ice mass over self weight at different tower station heights - (b)Predicted ice mass(black diamonds) over the blade length. The blade mass (related to the blade thickness) is represented by grey diamonds.

- Asymmetric masses causing unbalance
- Increased edgewise and tower vibrations were observed
- Ice accretion affects the control system and this could lead to increased loads (yaw error, wrong pitch, etc..)
- Change in aerodynamics makes the pitch turbine operate in stall
- Natural frequencies can be changed and thus reasonance occur (mainly true for light and small blades)

On the other hand, icing can also reduce fatigue due to the following:

- Shut down of turbines due to icing events reduces the number of cycle loads
- Icing might increase the aerodynamic damping and thus diminish components vibrations
- Variable sped or two speed turbine will operate at lower rotational speed when iced, and thus this would also reduce the number of cycle.(Nevetheless, from the previous listing the amplitudes of the loads would be higher.)

Given this two sides of the problem it seems that a detailled study should be performed to lead to relevant conclusions. For this, new standards are required and currently ellaborated[23]. Germanischer Lloyd describes in[23] different ice load cases that should be applied for fatigue analysis. For the case studied in this reference(a 2MW three bladed HAWT), the main load case was found to be the one corresponding to one blade iced and the other one being free. This results in an unbalanced rotor with a maximum (equivalent) load increase of 2.3% compare to normal conditions. It was found that the highest loads are obtained at rated wind speed and loads increases linearly with the duration of the icing event. This study also concludes that spetial measurements are suggested to get more certainty on the ice accretion phenomena and thus the assessments of loads and fatigue.

7.3.3 General conclusions

Analysis of WECO data and other sources led to the following observations:
Standard deviation of loads due to icing are:

- Reduced for flapwise bending moment
- Slightly reduced for edgewise bending moment

- Largely increased for the tower root bending moment

Power spectral density amplitude evolution due to icing:

- Flapwise bending moment: reduced at 1P and no other significant changes
- Edgewise bending moment: increased by a factor of five!
- Tower base bending moment: increased at 1P and at the first tower natural frequency
- The presence of ice decreases the natural frequencies

Loads observations

- Dangerous ice induced tower vibrations were found at wind speeds below stall.
- Extreme stall induced edgewise blade vibrations were found

Aerodynamic coefficients

- The aerodynamic penalty due to icing is primarily a function of the ice shape and size near the leading edge of the airfoil. Despite the icing following the airfoil shape, increase in drag coefficient and reduced lift is observed, which will imply reduced power output.
- The zero lift angle of attack increases with icing
- The drag coefficient increase with ice accretion

Power control

- In case of a pitch regulated wind turbine the rated speed is in general postponed due to the inhibition of the sensors on which the controller relies on.
- The rotational speed of the rotor could be affected by icing in the case of full variable speed.

The particular case of the lift coefficient The ice accretion increases the chord length, and this can increase the bending moments and pitching(torsional) moment at the blade root (During the WECO projects 66% increased in the bending moment at 3m/s and increased of 150% to 200% of the torsional moments for $\lambda = 6$ and $\lambda = 4$). However the effect of increased chord could be compensated by the decrease of lift coefficient due to the leading edge ice accretion, and thus no direct conclusion could be drawn. Nevertheless, the change in mass repartition will also induce bending moments and torsional moments.

7.4 Icing prediction

In order to asses the energy losses due to icing in the design of a wind farm, it is important to have an insight of the number of days per year with icing events. The WECO projects[56] realized an European icing map[58] which was the first attempt of the kind to describe icing Europe. The Icing map was produced using data from about 120 synoptic observation stations operated by national weather services. The final results shown on Fig. 7.8 gives a good insight of duration of icing events, intensity of rime accretion and variation of in-cloud icing with height above the sea level at various parts of Europe. The ice map combined with the European Wind Atlas is a proper tool for more precise prediction of annual energy production. Unfortunalty, no such map was found for Greenland. If no such map is available, and for direct use on field, the assessment of icing events can be done from temperature and the probability of icing with respect to temperature. Such informations could be used for controller design for instance. An idea of probability of icing occurring with respect to temperature is shown on Fig. 7.9. Between 0 and -12°water particles are in majority whereas in the range -21°to -40°, ice particles prevails. As ice particles will not create icing, the maximum probability is expected to be found between -4 and -8°. according to [8], relative humidity is not a representative parameter for assessing icing hazards for wind turbines.

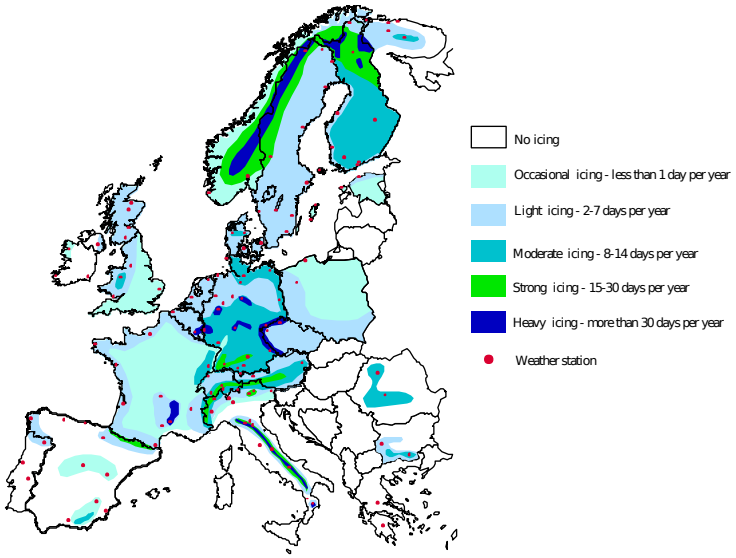

Figure 7.8: European Icing map[58]

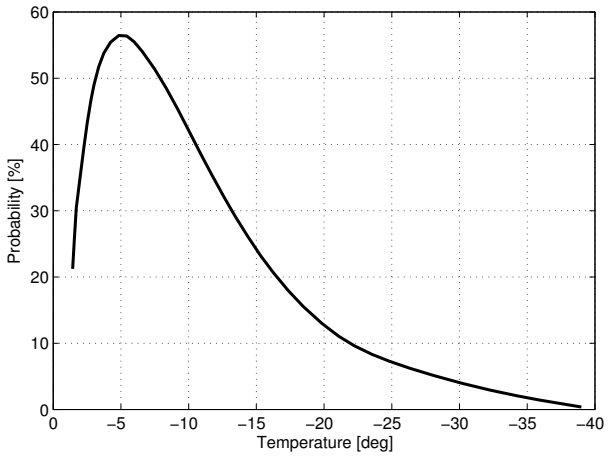

Figure 7.9: Probability of icing occurring versus temperature. Data obtained from observed cases.

Icing and anemometry Ice accretion on a cup anemometer increases the inertia and the drag and thus causes lower rotational speed. Small amount of ice can reduce significantly the measured wind speed(easily 30% underestimate), and large ice accretion can stop the anemometer (see Fig. 7.10). The influence of ice thickness has been studied experimentally[59] and theoretically[31]. Results from the later are presented in Tab. 7.1 but it should be noted that the degree of the underestimate varies strongly form region to region[59]. This is of course problematic for wind climate analysis, but can have dramatic influence on the control system in the case of a pitch regulated turbine. For instance, an iced wind vane will give false yaw error and this will result in energy losses. Also for a pitch regulated turbine, the wind turbine will not start if the anemometer display a wind speed lower than the cut in wind speed.

Table 7.1: Wind speed reduction on cup anemometer due to ice thickness[31]

Ice thickness [mm]	Speed underestimate [%]
0	0
0.5	12
1	33
2	37
4	49

Figure 7.10: Vane covered by ice (source EUMETNET [20]

7.5 Safety

7.5.1 Ice throws

During operation, fragments of ice from the rotor can be thrown off the turbine due to aerodynamic and centrifugal forces. During standstill and idling, it is mainly gravity that will make ice fragment to fall on the floor. This of course rises a question of safety for people passing by the turbine, housing, maintenance staff, electric lines, roads, etc. The distance and probability of ice throw is thus of prime importance. It will depend on the geometry of the ice fragment, the rotor azimuth, the rotational speed of the rotor, the local radius and the wind speed. Observations show that most ice fragments breaks off immediately after detaching from the blade and thus hit the ground into small fragments[19], either when the turbine is operating or not. The most dangerous zone is the one below the turbine because it is where the most ice throws occur. A picture of an ice fragments that was detached from a blade and hit floor is shown on Fig. 7.11a. A typical ice throw calculation would lead to a definition of an area that could be superimposed on a topographical map for all different wind directions. This area would typically have an ellipsoidal form, which depend on the wind speed and the tower height[19] as seen on Fig. 7.11b An area representing the risk can be estimated by simulation or by guessing a big circle around the wind turbine. To introduce this risk circle, the following empirical equation can be used:

$$d = 1.5\,(D + H) \tag{7.3}$$

with d the maximum throwing distance, D the rotor diameter, and H the hub height. For ice falls during standstill, the wind speed is a main parameter, and the following empirical equation can be used for the risk circle:

$$d = \frac{U}{15}\left(\frac{D}{2} + H\right) \tag{7.4}$$

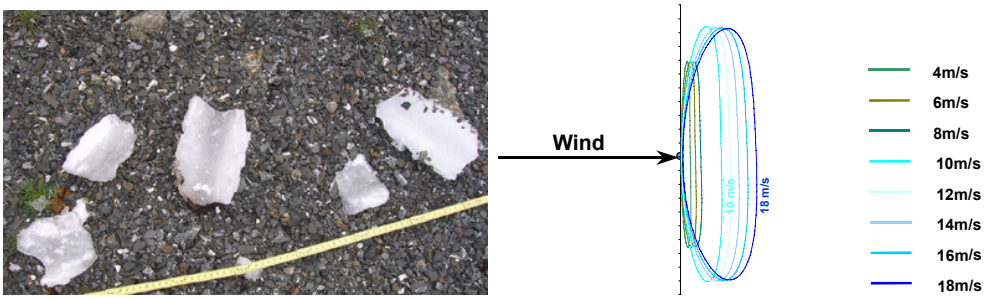

(a) (b)

Figure 7.11: Ice throws. (a) Photo of ice fragments [11] - (b) Results of ice throw calculation[19]

with U the wind speed at hub height. Nevertheless, in an experiment[11] carried out in the Swiss Alps it was found that this distance was never reached. In such a mountainous site(2300 m. asl), it was found that ice throws could also happen in summer. It is interesting to note that no relationship was found between the mass of the fragments and the throwing distance.

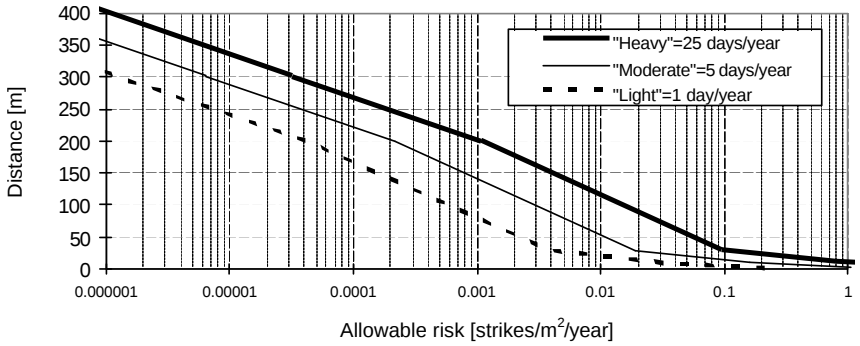

Figure 7.12: Safety distance at different icing levels for a 50m rotor[42]

7.5.2 Noise

Ice accretion increases the blade surface roughness and thus noise emission form the turbine. A shift of frequency to higher level is often observed.

7.6 Economics

7.6.1 Energy production

The energy production will be affected by icing which deteriorate power performances when the turbine is operating and which also imply more wind turbine stops. The deterioration of power performances includes the reduced power outputs in icing conditions, but also power oscillations. The effect of icing can be about 1 to 10% in light icing areas, but can go up to 50% in heavy icing area. The total time of ice presence on the blade has to be taken into account in power estimation. The icing event might be short, but if the temperature stay below zero for a long time after that, the ice is of course likely to stay on the blade. Also, icing events are often associated with high wind speed, which could hypothetically be harvest. The presence of ice imply thus even more losses in the total energy production due to low efficiency when good wind potential is present. Eventually, taking safety into account, the turbine might have to be shut down to reduce the risks of ice throws.

Part III

Overtaking the challenges of arctic conditions

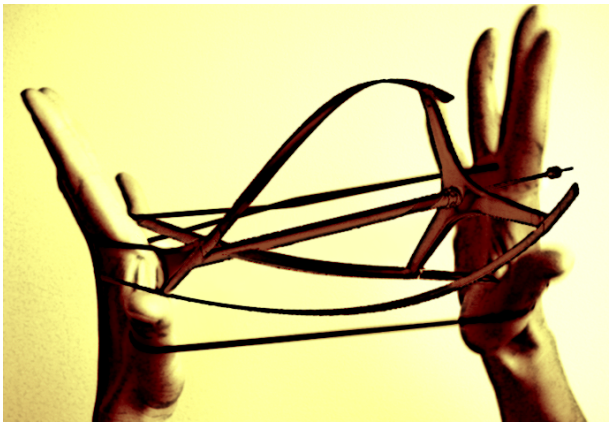

Chapter 8

Solutions and recommendations for cold climate sites like Greenland

8.1 Ice prevention techniques for wind turbines

In this section, solutions answering to the problem of icing affecting wind turbine rotor and anemometry are presented. The aim of an ice prevention equipment is to ensure continued, safe and economic operation in icing conditions. In most severe conditions such as Greenland, it is recommended to opt for solutions of complete evaporation of all impinging water.

Classification of systems In the following several systems of anti-icing and de-icing will be presented. The former prevent the formation of ice and has to be used continuously, whereas the latter allow ice to build up and then remove it operating thus in a cyclic way. These systems can also be divided into active and passive systems depending on their requirements in energy supply. Eventually, several fundamental method are found, mainly mechanical and thermal ones. The main systems, namely electric heating, hot air heating and inflatable rubber boots will be described in the following sections.

8.1.1 Thermal systems

Electro-thermal systems are active continuous anti-icing systems. They all require a control system with temperature sensors, a source of electrically generated heat and a distribution system. Two strategy can be chosen, either providing just enough energy to prevent the surface from freezing, running-wet strategy, or supplying sufficient heat to evaporate all water on the surface:evaporative strategy. For the first strategy, the water running beyond is likely to freez, creating “runback ice“ and thus reducing the power performances. Among all the systems used for anti-icing, the thermal solutions are the most energy consuming requiring high power densities.

Leading edge electric heating

In this system the leading edge is heated with electric power passing through foils of carbon fibers of metal. The first research activities were done at the VTT Technical research center(”Valtion Teknillinen Tutkimuskeskus”[67]) in 1992. In 1996, the Kemijoki Arctic Technology (KAT) published a the first commercial blade heating system, the JE-system[47], partly investigated during the WECO project. The basic scheme of such device can be seen on Fig. 8.1. In slight rime conditions(Fig. 8.2a) the heater will have an effect which even more extended than the heated surface, but this will not be the case for more severe situations(Fig. 8.2b). Numerical simulations from complex mathematical model[14] are carried out for further investigations of efficiency and design.

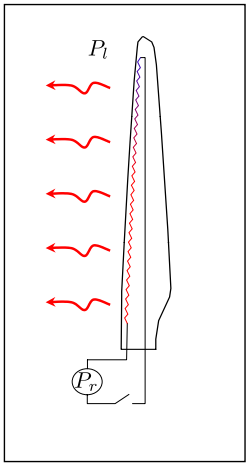

Figure 8.1: Leading edge electrical heating of a blade - Scheme

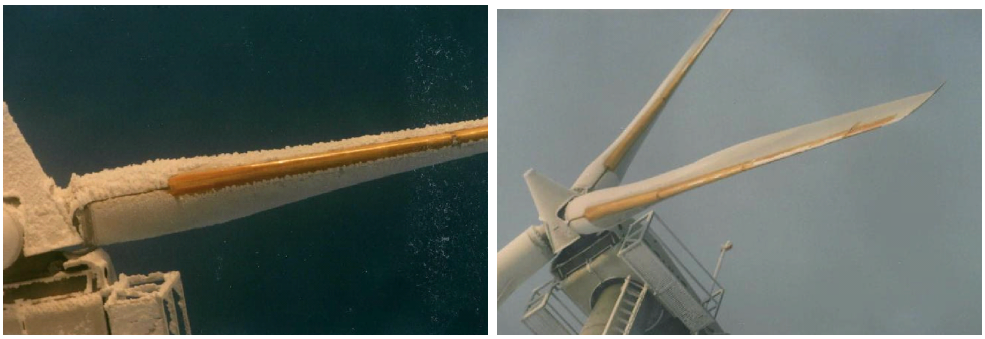

(a) (b)

Figure 8.2: Leading edge electrical heating of a blade - Pictures[35]. (a) Severe icing - (b) Slight icing

Operating conditions and control types Different heating strategies should be considered for stall regulated wind turbine. This is illustrated on Fig. 8.3 from [62]. In standstill and idling conditions, the heating system will melt the ice exactly where it mostly aggregates for a pitch controlled turbine. The turbine will thus be able to start operation. On the contrary, stall regulated turbines will accumulate ice on the side of the airfoil and will have difficulty to start at moderate wind speeds. Illustration of these differences can be found on Fig. 7.1.

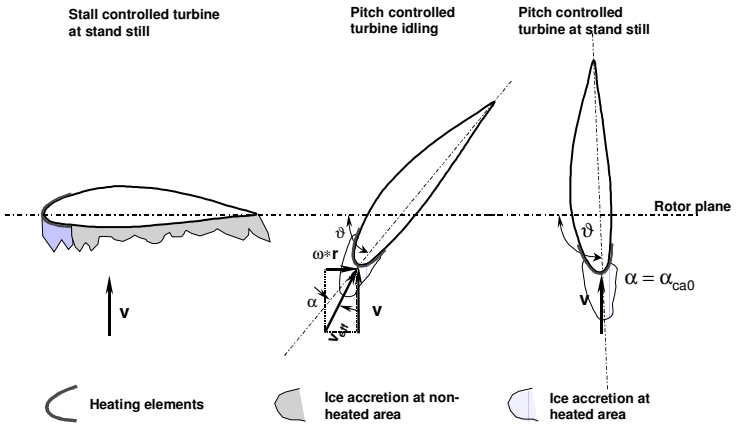

Figure 8.3: The need of a different strategy for stall wind turbine[62]

Proportion of power Such system requires a careful balance of the distributed heating power. Performances improved over the year, with now requirements of 1-3% of the rated power compared to values that used to be of 6%.

Cons In the down side, the presence of metal along the blade, makes the blade more likely to undergo lightning strikes. Nevertheless, real case study shown that the system did not suffer any damage from lightning strokes. The position of the heading elements imply stronger edgewise loads due to gravity.

Hot air circulation system

Two basic principles of hot air circulation system can be found depending if the flow is open or closed as illustrated on Fig. 8.4. The heated air from the heat source is conducted inside the leading edge of the rotor blade where it either flows back to the root inside the blade flange or flows up to the blade tip. Thew advantage of this method is that is does not modify the aerodynamics of the blades and does not attract lightning. On the other hand, the efficiency is reduced to the good thermal resistance(insulation) of the composite materials of the blade wall, and due to the high winds acting on the blade which cools it down by convection. The heating power has thus to be rather high to allow an evaporative process. Also, if ice is already present, this devise will not be able to remove the ice(de-icing). Two solutions are then found to improve the efficiency of the system: either increasing the thermal conductivity of the walls, either by spreading the applications points with local electrical pads along the blade.

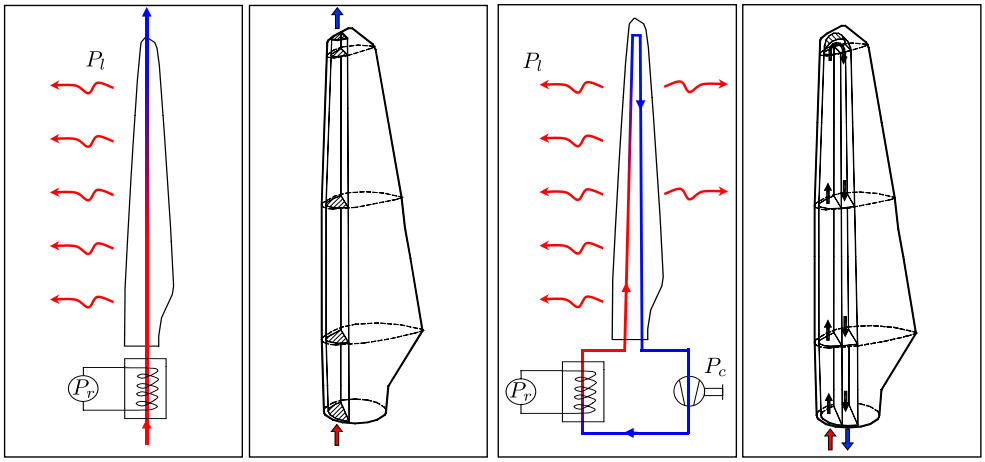

(a) (b)

Figure 8.4: Hot air circulation system. (a) Open system - (b) Closed System

8.1.2 Mechanical systems

Mechanical systems used to remove ice are based on mechanical shocks, forced vibrations, electromagnetic impulses, ultrasounds, electro and magneto-strained envelopes,and changes in the alloy memory. The resulting mechanical shocks will break the ice cap. These methods are thus intrinsically active(requires power) de-icing cyclic method.

De-icing boots on the leading edge

Inflatable rubber boots can be placed on the leading edge of the airfoil in order to act as a active de-icing system. When not operating, the vacuumed rubber tubes lay flat and conform to the profile shape on which they are applied. After the ice builds up to 6 to 13mm, a compressor activates with centrifugal force inflates the rubber tubes. This will imply stresses in the ice which will progressively break apart and be blown away by centrifugal force. Several cycles of inflations are needed to completely de-ice the blade. An illustration of such system can be found on Fig. 8.5. Such technology will nevertheless reduce the aerodynamic performances due to the profile alteration where it lays, and will imply additional noise.

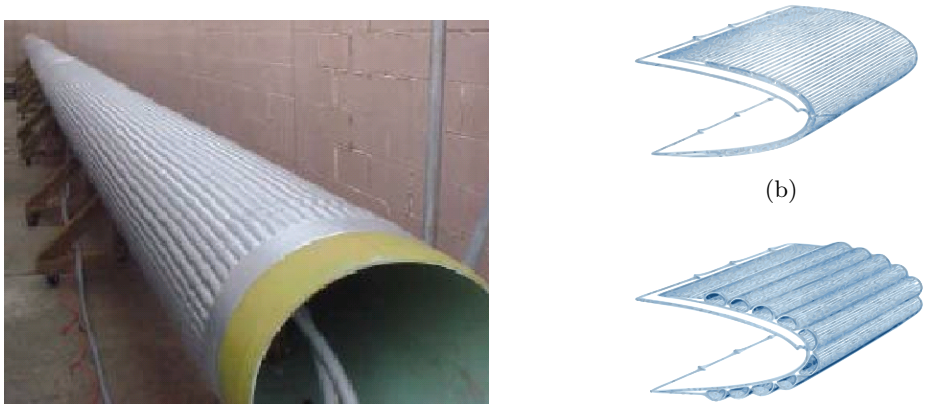

(a) (b) (c)

Figure 8.5: De-icing boots on blade's leading edge . (a) System implemented on blade - (b) Scheme of flat boots - (c) Scheme of inflated boots

8.1.3 Systems other than thermal and mechanical

Systems that does not involve heating or mechanical removal of the ice, can be based on solar radiation absorbent coating, hydro-phobic and ice-phobic coating, viscous products and greases. In general, these passive techniques do not always hinder ice formation, but help to limit its problematic effects. The advantage of these technologies is of course the easy implementations as it only consists of a chemical applications. This will consist in low cost solutions that does not imply lightning protection. The whole surface is protected and the maintenance is easy.

Special Coating

Special coating can be found that reduces the shear forces between the ice and the blade surface, and thus avoiding ice adhesion. An easy calculation can be made to assess the adhesion strength required for ice to shed spontaneously due to the centrifugal force $F_c = \omega^2 rm$, where m is the mass of ice equal to $m = \rho At$, with $\rho = 700\text{kg/m}^3$, A the element blade area at the radial position r and t the ice thickness. Using a rotational speed of $\omega = 2\text{rad/s}$ and a thickness of 20cm, the minimum adhesion strengh in the best conditions (tip speed and important mass):

$$\left.\frac{F_c}{A}\right|_{\text{tip}} = \rho t r \omega^2 \approx 18\text{kPa} \tag{8.1}$$

A material with adhesion strength below this value should be found, but as shown on Tab. 8.1, this will be a difficult task.

Table 8.1: Adhesion strength of ice for several material at -10°[8]

Material	Adhesion strength [kPa]
Steel	900
Epoxy paint	400
PVC	90
Teflon	40

Such coating should also have hydro-phobic and ice-phobic properties. Painted silicon cover material has good ice repellent properties, but after quite a short period on operating turbine blade it becomes porous and not ice repellent any more. Moreover this technology is not sufficiently to prevent ice and some some coatings can be toxic or corrosive.

Black painting

At low latitudes, where lots of solar energy is available, the effect of icing can be decreased by using blades painted black. During the day the blades would absorb solar radiation and the warmth of the blades will melt the ice, if the amount of ice is small. During the night though, the black blades will be iced at the same degree than blades of other colours. Also, in summertime the temperature of the blade's surface may affect the material properties of the glass fiber reinforced plastics (GRP) which is sensible to high temperatures. The idea of heating and using black painting has been used for wind measurements since the 1980's [60]. The gain for wind energy is in average really limited even in winter. An example oif black painted blade is seen on Fig. 8.2

Figure 8.6: Black coated blade with ice shedding[35]

8.1.4 Method comparisons

Comparison of the different method is delicate due to the difference of way of acting of each method. Also, one should take into account the energy gain due to the efficiency of the de-icing devise, and the economical perspective. Results from a comparative experiments[8] will be presented here without further description. In order to compare the anti-icing and de-icing methods, a comparative factor has been calculated from the ratio of energy required to remove 3 mm of ice to the value necessary for its fusion. Results are shown on Fig. 8.7

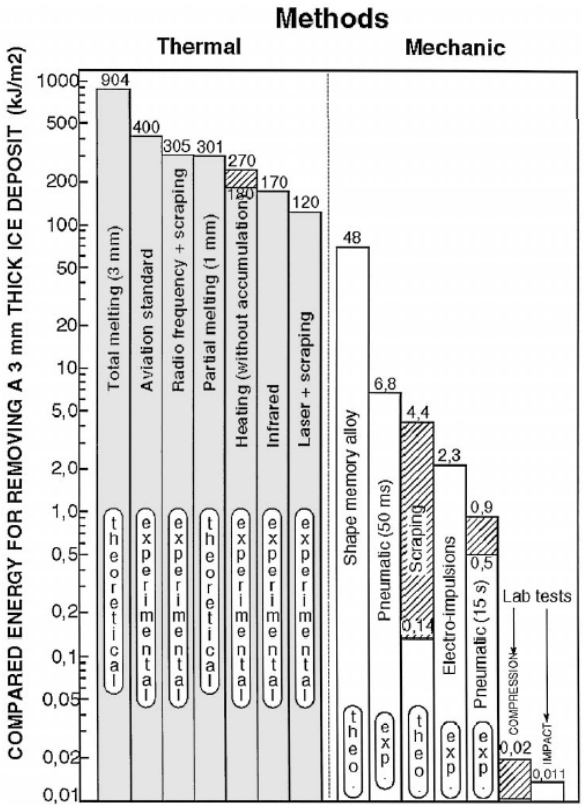

Figure 8.7: Comparison of the thermal and mechanical methods used for ice prevention[8]

8.1.5 Solutions for anemometry

The different class of icing for anemometers are the following:

0. Sensor totally free of ice
1. Ice on body and pole but not on the measurement element
2. Ice also on the measurement element
3. Sensor totally blocked by ice

At present there is a need for improved wind gauges designed for heavy icing conditions. Among the models available on the market few of them can survive harsh icing conditions and they could be sensible to slope winds thus indicating too high wind speeds in these conditions[59], and tilt effect which is typically observed in mountainous areas.These effects could lead to errors up to 10-12%.

The Eumetnet[20] project, mainly carried out in 2000/2001 by the Finnish Meteorological Institute[21], consisted in a review and testing of ice free anemometers at three different locations: Luosto(Finland, 515 m.a.s.l), Mont Aigoual(France, 1567 m.a.s.l) and Mont S antis(Switzerland, 2490m.a.s.l). A numerous amount of sensors have been tested with a list available online[20], amopng which the following models(heated version): Waa251, Waa252, Was425, Metek USA1, Gill, Wav252. The main manufacturers being: Visala, Degreane, Metek, Laumonier, Meteolabor. An example of such site, with ice free anemometer is shown on Fig. 8.8. Several recommendations and results from this study can also be found in[57].

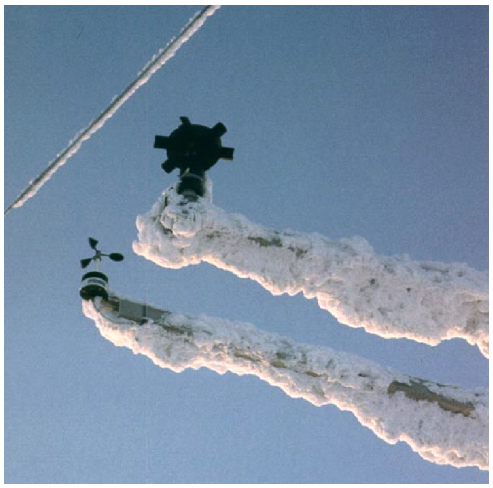

Figure 8.8: Testing of ice free anemometers within the EUMETNET SWS project

8.2 General recommendations for wind energy in cold climate

In this section a list of various recommendations is presented. These recommendations should be kept in mind when design a wind turbine for a cold climate site, and when wind measurement are performed in such environment. These recommendations recall the challenges of cold climate presented in chapter 5.

Field measurement

- As a general recommendation, wind measurement for wind power estimation in complex terrain should be more sophisticated in terms of instrumentation and technology.
- If no ice detector sensor is available, a thermometer and humidity sensor can be used alternatively.
- Ice free anemometers should really be used for reliable measurements even in slight icing conditions
- When temporary masts or remote sensors are used, at least 48 hours of wind data should be found in each wind direction sector to have reliable results. In general a data availability of 95% is required.
- Several masts are required for a better understanding of the flow, and measurements at several heights are important for assessing the vertical wind profile and it's dependency on wind sectors.
- Numerical or physical models should be combined to the field measurement to obtain an accurate wind resource estimation and thus an accurate power production assessment.
- Information about existing icing events should be retrieved for project development

Rotor

- Heated blades for extreme or frequent icing conditions are required

Ice throws In case of a significant risk for the public and operational staff several measures should be taken, like stopping of the turbine by the controller, or use of warning signs alerting anyone in the area(see Sect. 7.5.1), or implementing special turbine features to avoid ice accretion(see Sect. 8.1).

Component design Heating systems are required for control system, gear box and hydraulics and possibly other components within the nacelle (yaw system). Suitable lubricants for main bearings, gearbox, generator bearing should be used, and special oil for hydraulic system. Cold resistant steel for all structural members with welds (mainly the tower). Manufacturers often offer to add an optional cold weather package to a given wind turbine model which would typically include[8]:

- Heaters: in the gearbox, generator, control cabinet, nacelle
- Nacelle sealing
- Special alloy: ductile iron for hub and machine frame, tower steel
- Low temperature lubricants
- Heated anemometry
- Ice detectors
- Diagnostic package

References Probably the most complete and advanced references for recommendation on wind energy in wind climate would be the dedicated VVT working papers, which content is also found in several IEA reports[28]:

- VTT - Working paper 151: Expert group study on recommendations for wind energy projects in cold climates[65]
- VTT - Working paper 152: State-of-the-art of wind energy in cold climates[55]

Chapter 9

The use of vertical axis wind turbines

For high power productivity, the use of horizontal wind turbine(HAWT) is widely spread due to its efficiency and also its profitability for large scale turbines. Vertical axis wind turbines(VAWT) was not considered as being a potential for large wind farms since the 1990's. Research in VAWT has thus declined, but a regain of interest is seen lately with smaller scale applications for remote locations or small power systems. The question of VAWT versus HAWT does not have a black and white answer. In this section VAWT will be presented as it might be an adequate solution for the powering low energy telecommunication towers in Greenland. Another motivation is also the curiosity for these technology that was not part of any the DTU wind energy master courses.

9.1 Brief presentation of vertical axis wind turbines

9.1.1 Presentation

Vertical-axis wind turbine (VAWT) consists of a a vertical shaft around which the blades rotate. Such devices have been historically used hundreds of years BC for water pumping. The most famous design of VAWT differ from the way the extract energy from the wind. The Savonius wind turbine uses the drag force to rotate whereas the Darrieus type uses the lift. These two main design can be seen on Fig. 9.1. Most designs of VAWT inherits from these design. Lately, regain of interest has been found for the Darrieus kind of turbine which has an H shape. Solutions combining the two method of wind extraction are the split Savonius or Savonius/Darrieus design. As mentioned above, both HAWT and VAWT are proved by experience to work positively as

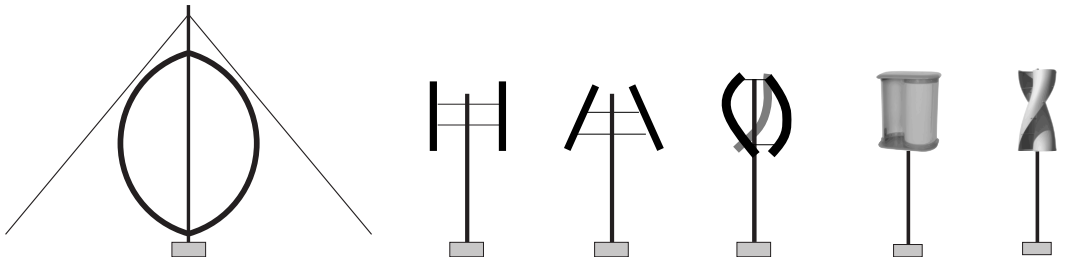

Figure 9.1: Vertical axis wind turbine. (a) Different design of Darrieus wind turbine - (b) Savonius designs

wind energy generators. Depending on the design constraints, one solution can be chosen versus the other. The feasibility of large VAWT wind farm has not proven efficient enough yet to compete with HAWT. As an anecdote though, it should be noted that Eole, the 4 MW vertical-axis Darrieus wind turbine constructed at Cap-Chat, Quebec, Canada, in 1988, operating during 6 years, was still holding this year the record of the largest-longest-running wind turbine. The first 5MW HAWT was implemented on 2005, and it will soon pass in front of the Eole turbine,

not to mention the 7.5MW Enercon turbine installed this year with the conventional expected life time of 20 years.

It is thus important to understand the pros and cons of each system, to decide with an economical; perspective as well, which design to use. Vertical axis turbines have several advantages over the typical horizontal axis turbines that can turn to be efficient to make a choice in some situations:

- Generator can be on the ground for more easy access, rather than up in the air
- Lower susceptibility to cross-winds
- Produces a torque around the vertical axis
- (No yaw mechanism needed)
- (Are more quiet)
- (Generally starts up at lower speeds)

The main disadvantages of vertical axis wind turbine are the following:

- Lower efficiency
- Requires bigger swept area
- Others, depending on the model. (often: material cost ,support, bearings, fatigue, startup, and speed control)

The range of efficiency, or maximum efficiency of the different types of wind turbines is well known as displayed on Fig. 9.2, where the clear advantage of horizontal axis wind turbines is seen.

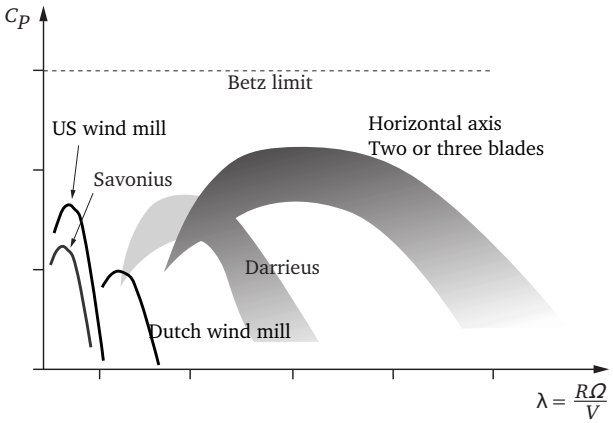

Figure 9.2: Power performances of the different kind of wind turbines

9.1.2 Motivations to use VAWT for Greenland

In the prospect of installing wind turbine for partially powering telecommunication tower in Greenland, the following main requirements are found:

- Reliability: The towers being remote, the system should be as autonomous as possible, and should not require too much maintenance. The simplicity of VAWT design like the Savonius one, goes in favor of this arguments. Several Darrieus turbine of the 1990 from the manufacturers FloWind and Adecon are still producing, proving the functionality of such devise. Nevertheless, not enough experience in Arctic conditions is found.

- Resistance to Greenland Harsh climate. Telecommunication towers being placed on top of hills, extreme wind can be found at these locations(up to 70m/s according to Telegreenland). Several VAWT design have cut-out wind speed up to 40m/s. In case of failure of the yaw mechanism, an HAWT could withstand really strong loads. Concerning the resistance to icing, no analysis were found, but in all case an anti-ice heating system would be required to resist Greenland cold climate.
- Low and simple maintenance: The generator being placed on the ground, VAWT allow an easier maintenance. The absence of pitch or yaw mechanism is also a plus for VAWT. Nevertheless, Small scale HAWT can also use a self orienting yaw mechanism.
- Among the recommendations of telegreenland, one mentionned "no slip rings", which is ones again in favor of VAWT due to the absence of yaw meachnism and the generator being placed on the ground.
- Strong structure and materials for the blades. The wind turbine should be able also to hit any ice build up on the mast.

Given the above constraint and requirements, the choice would probably go towards a Savonius rotor, which is the solutions used whenever cost or reliability is much more important than efficiency. The best is of course to do a comparative experiments with three different design consisting of a Savonius, A H-type Darrieus (helical or not) turbine, and a horizontal axis turbine placed in a location similar to the one were the telecommunication towers are placed.

9.2 Basic aerodynamics of Darrieus rotor

9.2.1 Introduction

The basics principles of Darrieus rotor is rather simple. Figure 9.3 represent the different velocity triangle composed by the wind velocity U_0, the relative velocity of the blade ΩR, so that by assuming that the wind direction and amplitude stay constant through the rotor, the determination of the relative wind seen by the blade is:

$$V = U_0 + \Omega R \tag{9.1}$$

The problem of such rotor, is that when stopped, the angle of attack are very high on the profiles so that the lift force is not efficient to make the rotor start. The torque is thus really low at startup, often preventing the turbine to rotate. This can be helped by adding a Savonius rotor on the shaft as a starter, because Savonius rotor have a high starting torque.

The power coefficient of a typical Darrieus turbine can be seen on Fig. 9.4 together with the torque coefficient as a function of the tip speed ratio. The maximum C_p is obtained for values of λ between 4 and 5

9.2.2 Litterature

Due to the limited amount of time for this report, the research knowledge provided by the following references could not be reported:[13] [5][4][54][68]

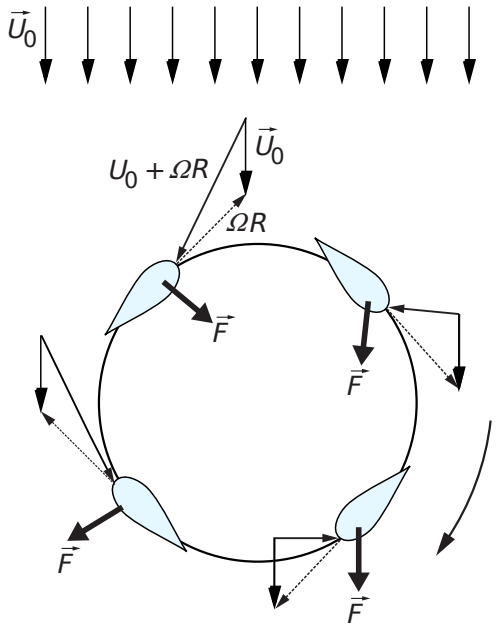

Figure 9.3: Scheme illustrating the different angle of attack encountered in one rotation

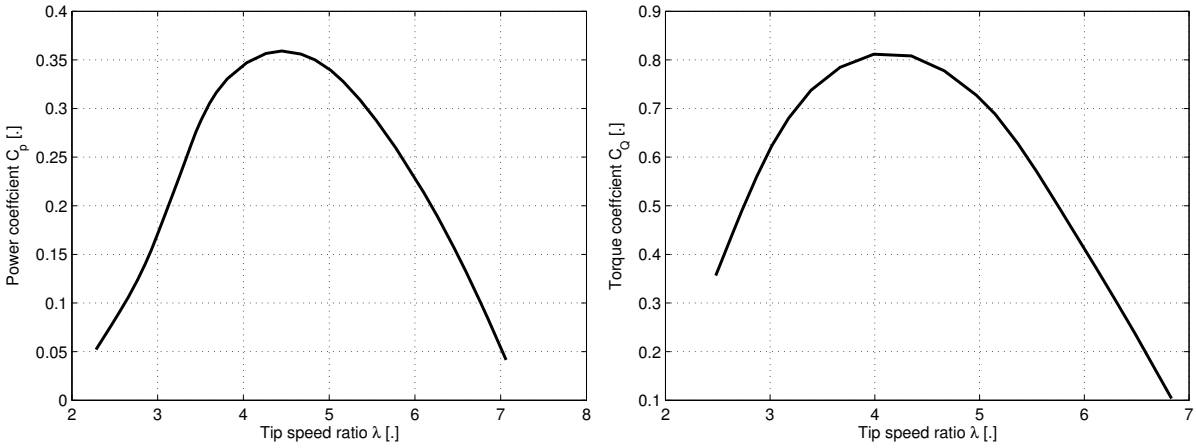

(a) (b)

Figure 9.4: Darrieus wind turbine performances. (a) Power coefficient - (b) Torque coefficient

9.3 Basic aerodynamics of Savonius rotors

9.3.1 Generalities

The classical Savonius rotor named after the Finnish inventor that patented it in 1931[52] has an “S-shaped“ cross section and appears as a vertical cylinder sliced in half from top to bottom. A scheme with the notations used for the description of the Savonius rotor is found on Fig. 9.5. s is referred as the (primary) gap spacing and a as the secondary gap spacing.

The principle of a Savonius turbine is based on the differential drag between each blade as seen on Fig. 9.6a. The subscript ”DH” will now stands for parameters related to the High Drag blade and ”DL” to the Low Drag blade. The design is improved compared to a cup anemometer by the fact that the air can circulate between the two half-cylinder which increases the torque. The flow passing between the two blades is indeed performing two succesives deviations of 180°and the pressure differences between the two sides of the resisting blade is reduced. This is illustrated on Fig. 9.6b. Each half cylinder is often refered as a “bucket”.

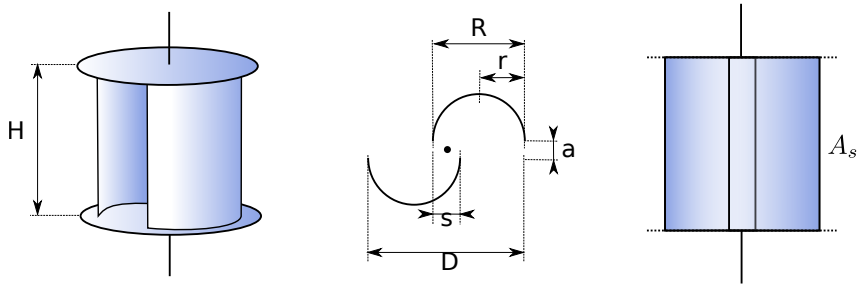

Figure 9.5: Scheme of the Savonius rotor. Dimensions and Swept area A_s

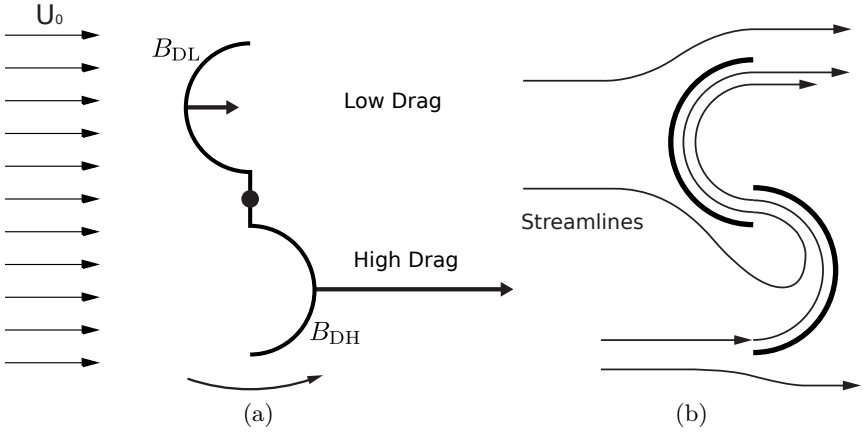

Figure 9.6: .

The starting torque of Savonius rotor is rather high compare to other design. This explains why it is often associated with a Darrieus rotor to provide the necessary torque for its startup.

9.3.2 Classical Savonius rotor - Performances definition

For the classical Savonius rotor the gap spacing s is nul and the blades have a cylindrical shape. For the following performances calculations it is further assumed that the flow is bi-dimensional hold in a cross section as shown on Fig. 9.7 and the frictional forces are neglected. Notations used for the following calculations are found on Fig. 9.5 and 9.7. For the Savonius rotor the tip speed ratio is defined as

$$\lambda = \frac{2\dot{\alpha} r}{U_\infty} = \frac{2\omega r}{U_\infty} \tag{9.2}$$

The steady state is assumed so that the rotational vector $\overrightarrow{w} = \dot{\alpha}\,\overrightarrow{k}$ is constant (i.e. $\dot{\alpha} = \omega =$ cst). For a given angular position of the rotor α, the instantaneous power is calculated from the torque which is the resulting of all the torque contributions of each infinitesimal element of the two blades:

$$P(\alpha) = \omega\, Q(\alpha) \tag{9.3}$$

$$Q(\alpha) = \int_{M \in B_{DH} \cup BDH} \left(\overrightarrow{OM} \times \overrightarrow{F}(\overrightarrow{M})\right) \cdot \overrightarrow{k}\; dM \tag{9.4}$$

For more convenience the torque is decomposed in the High drag blade Q_{DH} and Low Drag blade Q_{DL}:

$$Q = Q_{DH} + Q_{DL} \tag{9.5}$$

The actions on the blade are governed by the difference of pressure for each locations M_i on the blade. Let us consider that $\alpha = 0$ for simplicity of projections and describe the torque created

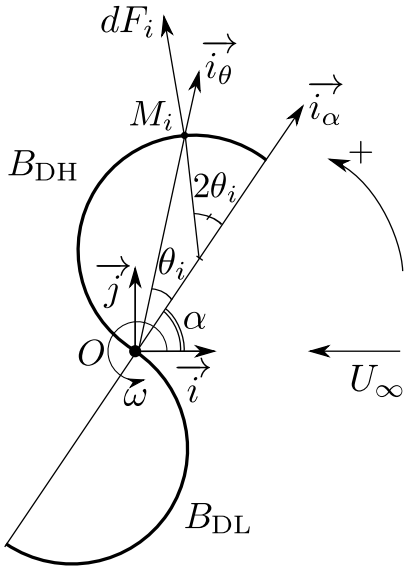

Figure 9.7: Notations used for torque integration

by an element of blade $dS = rH\,2d\theta$ located around the point M_i. The vectors involved are projected as:

$$\overrightarrow{OM_i} = r\left(\overrightarrow{i} + \cos 2\theta\ \overrightarrow{i} + \sin 2\theta\ \overrightarrow{j}\right) \tag{9.6}$$

$$\overrightarrow{dF_i} = dF\left(\cos 2\theta\ \overrightarrow{i} + \sin 2\theta\ \overrightarrow{j}\right) \tag{9.7}$$

$$\tag{9.8}$$

with $dF_i = \Delta p_i dS = \Delta p\, 2Hr\, d\theta$. The resulting torque for this force is thus:

$$dQ_i = (\overrightarrow{OM_i} \times \overrightarrow{dF_i}) \cdot \overrightarrow{k} = rdF \sin 2\theta = 2Hr^2 \Delta p_i \sin 2\theta \tag{9.9}$$

Gathering all the torque contributions of the two blades it yields:

$$Q(\alpha) = 2Hr^2 \int_0^{\pi/2} (\Delta p_{\mathrm{DH}} - \Delta p_{\mathrm{DL}}) \sin 2\theta\, d\theta \tag{9.10}$$

The knowledge of pressure distribution by experiments of simulation is now required to finish the calculation. Once these pressure differences are determined for all the rotor positions α the average power over a half rotation(enough due to symmetry) of the rotor can be eventually calculated with:

$$\overline{P} = \omega \overline{Q} = \omega \frac{1}{\pi} \int_0^{\pi} Q(\alpha) d\alpha \tag{9.11}$$

The total turbine swept area is defined as $A_s = 4rH$. It corresponds to the frontal area when there is no gap spacing s. This area is used to normalize the power and torque:

$$C_P = \frac{\overline{P}}{\frac{1}{2}\rho U\infty^3 A_s} \tag{9.12}$$

$$C_Q = \frac{\overline{Q}}{\frac{1}{2}\rho U\infty^3 A_s} \tag{9.13}$$

9.3.3 Classical Savonius rotor - pressure distribution

Experimental determination An experimental study of the pressure differences at 7 different locations on the blade and for all azimuthal angle α was realized by [12]. The results from this reference are shown on Fig. 9.8 with a figure translated in english borrowed from[45]. The pressure difference is expressed in term of pressure coefficient.

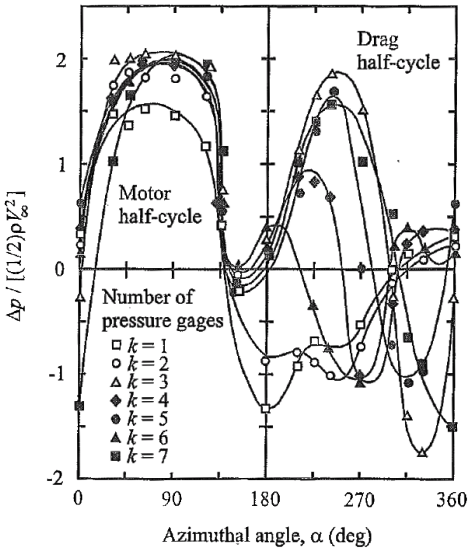

Figure 9.8: Differences of pressure coefficient at several location along the blade for the Savonius rotor

Model Despite the static assumption on the flow, the torque expression should take into account the rotation of the bucket. Due to the differences of drag between the motor half-cycle and the drag half-cycle, two different models are assumed[12] for the differential pressure coefficient. For the High-Drag half-cycle the difference of pressure is assumed to be dependent of the relative velocity $U_r = U_\infty - U_i$ with U_i being the velocity of a point on a blade. The low-drag half-cycle has an increased effect as the rotational speed increases, and there is thus a limit for which the rotor does not supply any power. It is thus suggested by[12] that the predominant effect for resistive half-cycle is due to the rotational speed only and not the incoming wind speed. The above discussion writes:

$$\Delta p_{\mathrm{DH,i}} = \frac{1}{2}\rho U_r^2 \times K_{\mathrm{DH}}(\alpha) \tag{9.14}$$

$$\Delta p_{\mathrm{DL,i}} = \frac{1}{2}\rho U_i^2 \times K_{\mathrm{DL}}(\alpha) \tag{9.15}$$

The function K_{DH} has values around 1.8 and can be approximated for instance with a sinusoidal function of α. Assuming that K is only a function of α, Eq. (9.10) can be further developed using Eq. (9.14):

$$Q_{\mathrm{HD}}(\alpha) = \rho H r^2 K_{\mathrm{DH}}(\alpha) \int_0^{\pi/2} U_r^2 \sin 2\theta \, d\theta \tag{9.16}$$

The expression of U_r^2 should be carefully derived. The velocity of a point of a blade is

$$\overrightarrow{U_i} = U_i \overrightarrow{j_\theta} \tag{9.17}$$

with $U_i = \dot{\alpha}\|\overrightarrow{OM}\|^2$. With a geometrical relation one can express $\|\overrightarrow{OM}\|$ as a function of θ and r:

$$OM = \frac{r\,(1+\cos 2\theta)}{\cos\theta} \tag{9.18}$$

To express $\overrightarrow{U_i}$ in the reference frame, two successive rotations are applied:

$$\begin{pmatrix} \overrightarrow{i_\theta} \\ \overrightarrow{j_\theta} \end{pmatrix} = \begin{pmatrix} C & S \\ -S & C \end{pmatrix} \cdot \begin{pmatrix} \overrightarrow{i_\alpha} \\ \overrightarrow{j_\alpha} \end{pmatrix} = \begin{pmatrix} C & S \\ -S & C \end{pmatrix} \cdot \begin{pmatrix} c & s \\ -s & c \end{pmatrix} \cdot \begin{pmatrix} \overrightarrow{i} \\ \overrightarrow{j} \end{pmatrix} \tag{9.19}$$

with uppercase letters representing the function cos and sin applied on θ and for the lowercase letters, applied on α. The norm of $\overrightarrow{U_r}$ can now be calculated as follow:

$$U_r^2 = (U_i\,(Sc + Cs) - U_\infty)^2 + U_i^2(Cc - Ss)^2 \tag{9.20}$$

The development of the previous equation will lead to four terms. Following Eq. (9.16), each of these terms are multiplied by $\sin 2\theta$ and integrated (Maxima[38] is of great help here), without forgetting to use Eq. (9.18) for the expression of U_i as a function θ, to eventually obtain the final expression:

$$Q_{\mathrm{DH}}(\alpha) = \rho H r^2 K_{\mathrm{DH}}(\alpha) \left(U_\infty^2 + 2\dot{\alpha} r^2 - \frac{\pi}{2} U_\infty \dot{\alpha} r \cos\alpha - 2 U_\infty \dot{\alpha} r \sin\alpha \right) \tag{9.21}$$

Equation (9.21) can be used to derive the torque for the low-drag cycle according to Eq. (9.15) by substituting $U_\infty = 0$, which leads to:

$$Q_{\mathrm{DL}}(\alpha) = \rho H r^4 K_{\mathrm{DL}}(\alpha) \dot{\alpha} \tag{9.22}$$

The expression of the torque being known with Eq. (9.21) and Eq. (9.22), the power is expressed as a function λ (see Eq. (9.2)):

$$P = \dot{\alpha} Q = \frac{1}{4} \rho A_s U_\infty^3 \left[K_{\mathrm{DH}}(\alpha) \left(\frac{\lambda}{2} + \frac{\lambda^3}{4} - \frac{\lambda^2}{8} \pi \cos\alpha - \frac{\lambda^2}{2} \sin\alpha \right) + K_{\mathrm{DL}}(\alpha) \left(\frac{\lambda^3}{4} \right) \right] \tag{9.23}$$

And the average power can then be calculated according toEq. (9.11).

Assuming constant K In this paragraph $K_{\mathrm{DH}}(\alpha)$ and $K_{\mathrm{DL}}(\alpha)$ are assumed constant and are respectively written K and K'. The integration of Eq. (9.23) according to Eq. (9.11) can be done and one obtains:

$$\overline{P} = \frac{1}{2} \rho A_s U_\infty^3 \left[\frac{K\lambda}{2} \left(\frac{1}{2} - \frac{\lambda^2}{\pi} + \frac{\lambda^3}{4} \left(\frac{K - K'}{K} \right) \right) \right] \tag{9.24}$$

or:

$$C_p = \frac{K\lambda}{2} \left(\frac{1}{2} - \frac{\lambda^2}{\pi} + \frac{\lambda^3}{4} \left(\frac{K - K'}{K} \right) \right) \tag{9.25}$$

The criteria $K' \geq K$ has to be added to ensure that a limit is found for which the rotor does produce power. Choosing $K = K'$ leads to

$$C_p = \frac{K\lambda}{2} \left(\frac{1}{2} - \frac{\lambda}{\pi} \right) = C_{p,\max} \frac{16}{\lambda} \pi \left(\frac{1}{2} - \frac{\lambda}{\pi} \right) \tag{9.26}$$

with $C_{p,\max} = K\pi/32$ obtained for $\lambda_{\max} = \pi/4$. Given the values from the experimental study found on Fig. 9.8 one gets $C_{p,\max} = 0.17$. The limit of power production is obtained for $\lambda_L = 2\lambda_{\max} = \pi/2$. The power coefficient obtained for a S-shaped rotor without spacing gap, given the hypothesis $K = K'$, with K independent of α, and given the hypothesis from Eq. (9.14) and Eq. (9.15) is found on Fig. 9.9.

9.3.4 Non conventional Savonius rotor

The typical power and torque coefficient for Savonius rotor with a gap spacing $s/d \approx 0.24$ is shown on Fig. 9.10. Such value of the gap spacing has been obtained by optimization of the static torque with numerical simulations[39]. This study advised a configuration with a rotor height of twice the rotor diameter $H = 2D = 4R$, a gap spaceing $s/d \in [0.15\ ;\ 0.3]$ with no secondary gap spacing. At least two rotors separated by 90°are recommended to allow starting($Q > 0$) in all directions (see Fig. 9.11b). Using more than two rotors, has only an interest to reduce the loads fluctuations as shown on the dynamic study [26].

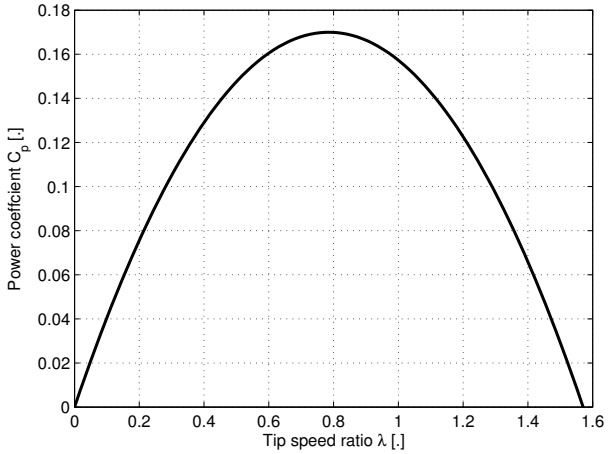

Figure 9.9: Theoretical Savonius power coefficient. The following are assumed: a S-shaped rotor without spacing gap, $K = K'$, with K independent of α and the hypothesis from Eq. (9.14) and Eq. (9.15)

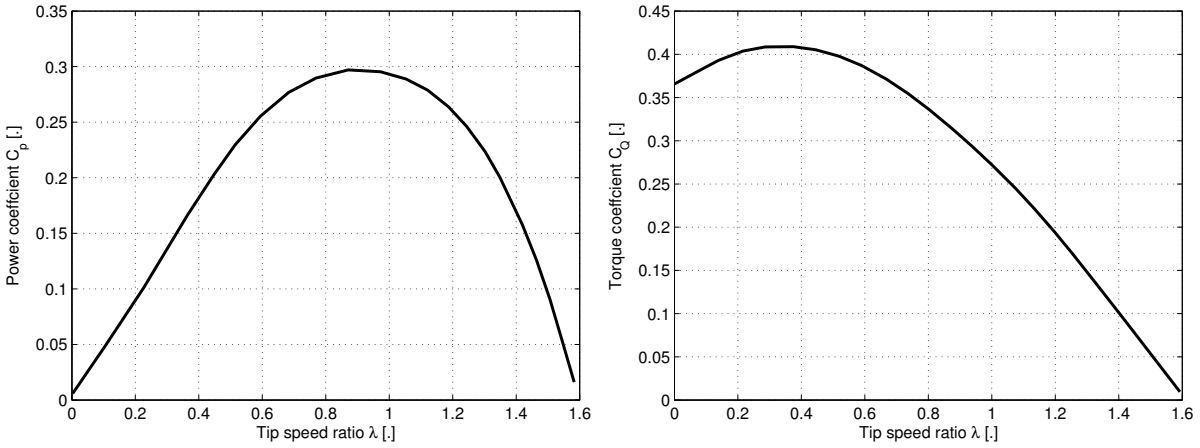

(a) (b)

Figure 9.10: Savonius wind turbine performances. (a) Power coefficient - (b) Torque coefficient

Static torque Despite the high starting torque of the Savonius rotor, it can be seen on Fig. 9.11 that there is a small range of wind angle for which the resulting torque on the two blades is zero. In such configuration, if the turbine is originally stopped, it will not start. This is often solved by a layout of two or more Savonius rotors on top of each other rotated by a 90°angle, so that the some of the two static torque is positive for all rotor angle, and thus the rotor can always start.

Performances Several solutions are envisaged to improve the efficiency of the Savonius rotor. The use of twisted blades is more and more spread, and so is its study[51]. A higher positive torque seem to be found and by changing the twist angle the rotor can be optimized for a given wind speed(large twist for low wind speed). The use of curtains[7] but this requires an mechanism to orient the curtains always facing the wind which is likely to add problems with icing conditions and also increase the wind turbine price.

9.3.5 Litterature

Due to the limited amount of time for this report, the research knowledge provided by the following references could not be reported :[37] [32] [22] [48] [46] [41] [12] [40] [49] [9]

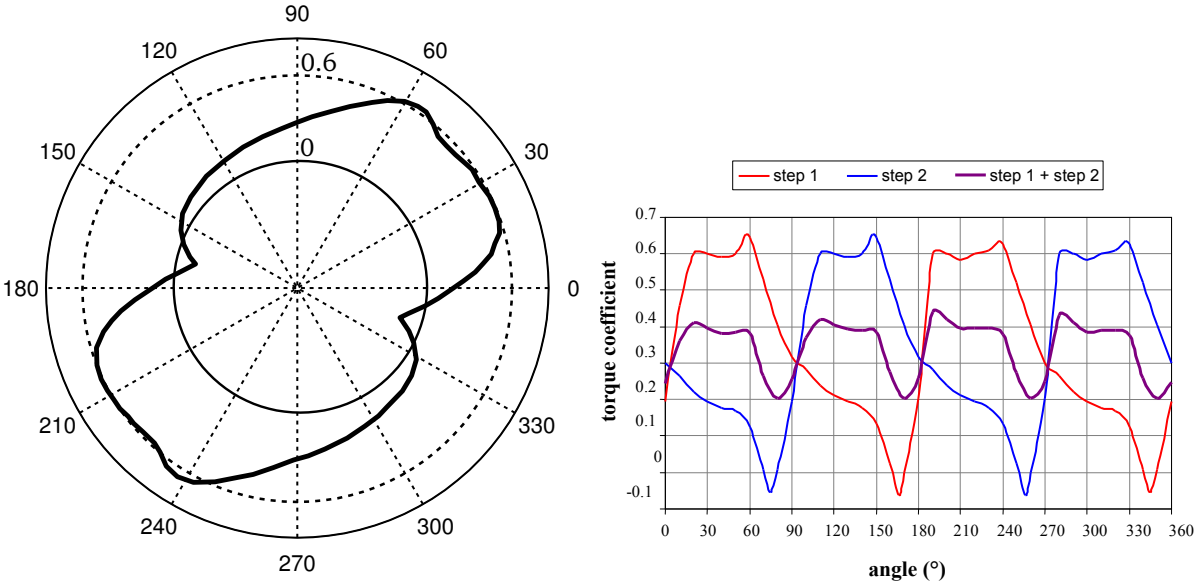

(a) (b)

Figure 9.11: Savonius rotor static torque. (a) Polar representation of Savonius turbine static torque as a function of the position angle of the rotor α - (b) Cartesian representation for two rotors individuals or associated

Part IV

Applications of wind energy in cold climate

Chapter 10

Existing cases of wind turbines in cold climate

10.1 Wind turbines in Cold climate

Fig. 10.1 from [66] shows the repartition of existing wind farms in cold climate. No point can be seen for Greenland, but there is and has been several wind turbines installed in Greenland. Several of them will be listed in the next section. Most of the turbines presented in Fig. 10.1

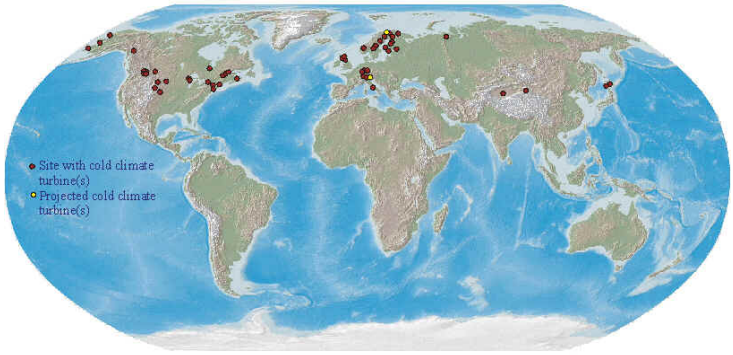

Figure 10.1: Repartition of wind farm project in cold climate - 1997 - Source[66]

are horizontal axis with power placed in mountainous areas with production ranging from few hundreds of kW to multimegawatt machines. Several prototypes from the former manufacturer Bonus(bought by Siemens) were used in the 90's for experimentation. Among others:

- Lammasoaivi wind farm, the first arctic wind farm in the world, constructed by Kemijoki Oy in 1996 with two Bonus 450 kW turbines and one 600 kW[3]
- Wind turbines at the top of Pyh atunturi Fell in Finland[17]. In 1993 a 220 kW wind turbine was erected, which was the first one with a JE blade heating system
- Appelbo wind turbine in Sweden 900W from NEG Micon[27]
- 600 kW Enercon wind turbine with integrated blade heating on G:utsch mountain, Switzerland, at 2'300 m asl [11]
-

10.2 Wind turbines in Greenland

Wind turbiens encountered during the projects The wind turbines from Assaqutaq consisted in a 100W Ampair PACIFIC HAWT, and a 108W Windside WS-015B PLUSS VAWT. According to report[63], that performed the first analysis of production of these turbine, the following conclusions were found:

> The solar panels and controller are working as designed. The vertical wind turbine seems to produce only during high winds and its energy contribution is insignificant. The horizontal wind turbine contributes power to the battery but provides readings that are not physically reasonable and creates noise on other components.

The advantages of Windside wind turbine is that the don't have cut out wind speed, and they are design to wiithstand high wind speed, up to 60m/s for class A wind turbines.

Wind turbine tried by Telegreenland Unfortunalty, few data are available concerning the different try done by Telegreenland, but from an exchange of email, it seemed that most of the 15 to 20 tries failed, and the one still standing require a lot of maintenance. A citation of this email exchange is provided below:

> Horizontal wind turbines:
> - WRSK 503 IND, 500VA, Nuuk, 2001 - 2004, ran out of production.
> - AIR 403, 400VA, Nuuk, 14 days, short circuit, electric fault. Replaced by AIR403-IND.
> - AIR 403-Marine, 400VA, ELFJ, 1 week, 2 wings flew away. produced 7 Ah.
> - H40, 1KW, 12 weeks, too much noise, moved to site SKIN,Âă lived 14 days.
>
> Vertical wind turbine:
> - VRE.005 , 500VA , Nuuk, December 2003, in April 2004 there was measured 40m/s. wings started to break apart.
> - VRE.007 , 750VA, Nuuk , summer 2004, stronger wings. Wings flew away during storm, 54m/s.
> - VRE.007, 750VA, Nuuk , summer 2005 , wings reduced to half size. Âă
> - VRE.3xxx, 3000VA, KIN, oktober 2006, 12 weeks, one wing flew away.
> - VRE 003, 100VA, UNOQ, TOP300, HOLM. 2 running today.

(a) (b)

Figure 10.2: Examples of wind turbine used by Telegreenland. (a) VRE.3xxx, 3000VA - (b) VRE.007, 750VA

Chapter 11

Feasibility of wind power applications for telecom

11.1 On the need of wind energy for telecom

On some sites operated by TELE Greenland (TG), the fuel cost for each kWH is around 50 DKK. This price includes the cost for the fuel and the transportation cost. An average TG site have a typical power consumption of around 1 kW. As a result of this, the total amount of money for one telecommunication tower per day is 1 kW x 24 H x 50 DKK = 1.200 per day and per year 438.000! A reduction of the cost could be obtained by introducing wind energy to these sites. Figure 11.1 Illustrates the telecommunication tower supported in fuel by helicopter, and undergoing harsh climate conditions.

(a) (b) (c)

Figure 11.1: The need of wind energy for telecom in Greenland. (a) Typical helicopter lift for maintenance material and fuel - (b) Telegreenland telecommunication tower - (c) Telecommunication tower covered by ice

11.2 Preliminary design recommendations

A 1kW generator from AXCO motors has been bought to be tried on a wind turbine applied for telegreenland. An illustration of the series of Axco generator is shown on Fig. 11.2. A design of wind turbine should be found to fit this generator. Providing the experience of Telegreenland, it seems that most of the time, the problem is in the robustness of the material used. The wind turbines tested did not withstand the extreme winds found at the telecommunication tower locations. Nevertheless, it seems that mostly Darrieus Type turbines were used, which are known to be subjected to strong fluctuating loads. A Savonius rotor, like the model WS-4 from Wind site could be a good starting point for a design adapted to Greenland and fit with the AXCO 1kW rotor bought by Ole B. Skipper A/S for this project. The swept area is nevertheless a little bit too small given the size of the generator. It should be multiplied by two, thus getting

Figure 11.2: Axco generator model for wind turbines

closer to the WS-12 model. The structure should be reinforced to withstand constant extreme winds not of 60 but 70m/s or more. These reinforcement should mainly concern the way the blades are fixed. The Windsite rotor design seem rather robust for this matter.

Conclusion

The recommendations presented in this report could be taken into account for implementing wind turbines in Greenland. Nevertheless, this would require several experiments and trial before a final design could be achieved. If a fast design is required to fit the AXCO generator of 1kW, then it is believed that a wind turbine such as the WindSite WS-4 or WS-12 would be a good start for a design. The company has indeed acquired quite some experience from wind energy in Finland that could be directly used for Greenland, providing maybe a reinforced structure. When enough experience would be acquired, a heating system should be investigated based on the solutions presented in this report in order to optimize the energy production by limiting the time of un availability of low efficiency due to icing. The main objective for this report was to learn about vertical axis wind turbine, and understand the challenges and solutions of icing related to wind energy. Indeed, vertical axis wind turbines are not taught at DTU and this project allowed to fill this gap. Due to a lack of time, little amount of informations was transmitted in this report concerning vertical axis wind turbines. Nevertheless, several publications and reference materials was read, and a more precise view of the topic was achieved. Moreover, this year 2010 exceptionally, the course Ice prevention techniques for wind energy was not offered at DTU. This report was for the author a way to get a grasp on this subject and to report it so that hopefully it could help and save time in any further field work applications related to wind energy in Greenland. Eventually, the field work itself in Greenland was a unique experience where a lot has been learn on measurements techniques, in a well organized frame with an effective and appreciable supervision from Kasper. On top of the scientific knowledge that this project brought, it was also a rich human experience in an amazing environment that made this whole trip a one-life experience.

Bibliography

[1] 12494, I. *Atmospheric icing of structures, First edition.* Geneva, August 2001.

[2] 3tier. *http://www.3tier.com/en/.* 3tier, 2010.

[3] Aarnio, E., and Partonen, S. *Operational experience of arctic wind farms.* BOREAS V, Levi, Finland, 2000.

[4] Abdel Azim El-Sayed, A., Hirsch, C., and Derdelinckx, R. Dynamics of vertical axis wind turbines (darrieus type). *Journal of Rotating Machinery 31*, 1 (1995), 33–41.

[5] Ajdehak, E. Analysing power generation in vertical axis wind turbines. Bilfinger Berger Services Australia, unpublished.

[6] Al-Khalil, K. M., Horvath, C., R.Miller, D., and Wright, W. *Validation of NASA Thermal Ice Protection Computer Codes Part 3:Validation of ANTICE.* NASA TM 2001-210907, May 2001.

[7] Altan, B., and Atilgan, M. An experimental and numericla study on the improvement performances of savonius wind rotor. *Energy conversion and Management 49* (2002), 3425–3532.

[8] Battisti, L. *Wind turbine operations in cold climates.* DTU lecture slides, June 2009.

[9] Blackwell, B., and Sheldahl, R. Wind tunnel performance data for two and three bucket savonius rotors. Tech. Rep. SAND76-0131, Sandia Laboratories, July 1977.

[10] Branlard, E. *Analysis of wind data for Greenland.* DTU, December 2010.

[11] Cattin, R., Kunz, S., Heimo, A., Russi, G., Russi, M., and Tiefgraber, M. Wind turbine ice throw studies in the swiss alps. Meteotest„ 2004.

[12] Chauvin, A., Botrini, M., Brun, R., and Béguier, C. Evaluation du coefficient de puissance d'un rotor savonius. *C.R. Académie des Sciences de Paris 296, Série II* (March 1983), 823–826.

[13] Cooper, P., and Kennedy, O. Development and analysis of a novel vertical axis wind turbine. University of Wollongong, unpublished.

[14] da Silva, G., de Mattos Silvares, O., and de Jesus Zerbini, E. Numerical simulation of airfoil thermal anti-ice operation - part 1: Mathematical modeling. *Journal of Aircraft 44*, 2 (March 2007).

[15] DMI. *http://www.dmi.dk/greenland.* DMI, 2010.

[16] Doerner, H. Efficiency and economic comparison of different wec-(wind energy converter) rotor systems. In *Appropriate Technologies for Semiarid Areas: Wind and Solar Energy for Water Supply* (1975), Proceedings of the Seminar Centre for Economic and Social Development (DSE), Berlin (Germany) - German Foundation for International Development.

[17] Durstewitz, M. European experience with wind turbine in icing conditions. unpublished, 2004.

[18] et al., G. R. Measures needed for the successful development of wind energy in icing climate. Unpublished, 2010.

[19] et al, H. S. *Risk analysis of ice throw from wind turbines.* BOREAS VI, Pyh a, Finland, 2003.

[20] Eumetnet. *http://www.eumetnet.eu/.* eumetnet, 2001.

[21] FMI. *http://ilmatieteenlaitos.fi.* FMI, 2010.

[22] Fraenkel, P. *Les Machines Elevatoires - Bulletin FAO d'irrigation et de drainage.* FAO - Bulletin 43,ISBN 92-5-202515-4, 1994.

[23] Frohboese, P., and Anders, A. Effects of icing on wind turbine fatigue loads. *Journal of Physics: Conference Series 75, The Science of making torque from wind* (2007), 1–14.

[24] García, C. *Heating of Tourist Cottage in the Arctic.* DTU-Artek, Center for Arktisk Technologi, 2009.

[25] Hansen, K. *http://www.winddata.com/Greenland.* RISØ-DTU, 2010.

[26] Hayashi, T., LI, Y., Hara, Y., and Suzuki, K. Wind tunnel tests on a three-stage out-phase savonius rotor. unpublished.

[27] Homola, M. C. Impacts and causes of icing on wind turbines. Tech. rep., Interreg IIIB Project - Narvik University College, 2005.

[28] IEA. *Wind Energy Annual Report 2009.* IEA - ISBN 0-9786383-4-4, July 2010.

[29] IPCC. *http://www.ipcc-data.org/.* Intergovernmental Panel on Climate Change, 2010.

[30] Jacob, D. J. *Introduction to atmospheric chemistry.* Princeton University Press, Harvard University, January 1999.

[31] Kimura, S., Tammelin, B., and Peltomaa, A. *Appendix in the final report of the EUMETNET SWS project.* Finnish Meteorological Institute, Helsinki., 1998.

[32] Leconte, P., Rapin, M., and Szechenyi, E. *Éolienne.* Techniques de l'Ingénieur - BM 4640, 2001.

[33] Levinson, L. H., Potapczuk, M. G., and Mellor, P. A. *Software Development Processes Applied to Computational Icing Simulation.* Lewis Research Center - NASA/TM1999-208898, January 1999.

[34] Mahmoud, A. *Wind turbine Proven6-300 Testing & Installation.* DTU-Electrical Engineering, 2009.

[35] Maissan, J. *Wind Power development in sub-arctic conditions with severe rime icing.* Circumpolar Climate Change Summit and Exposition, march 2001.

[36] Makkonen, L., Laakso, T., Marjaniemi, M., and Finstad, K. Modelling and prevention of ice accretion on wind turbines. *Wind Engineering vol. 1*, 21 (2001), 3–21.

[37] Martin, J. *Énergies éoliennes.* Techniques de l'Ingénieur - BM 8585, 1997.

[38] Maxima. *http://maxima.sourceforge.net/.* Maxima, 2010.

[39] Menet, J.-L., and Bourabaa, N. *Increase in the Savonius rotors efficiency via a parametrix investigation.* ENSIAME, 2004.

[40] Menet, J.-L., and Bourabaa, N. *Prévision des performances aérodynamiques d'un nouveau type d'éolienne à axe vertical : le rotor à contrevoiles.* XVIIIème Congrès Fra cais de Mécanique, August 2007.

[41] Menet, J.-L., and Ménart, B. *Une procédure de comparaison de quelques éoliennes classiques basée sur l'utilisation du critère l-sigma.* XVème Congrès Fra cais de Mécanique, September 2001.

[42] Morgan, C., Cossanyi, E., and Seifert, H. Assessment of safety risks arising from wind turbine icing. *EWEC 97 Proceedings, Dublin, Ireland* (October 1997), 141–144.

[43] NSIDC. *http://nsidc.org/.* National Snow And Ice Data Center, 2010.

[44] Panorama, V. F. *http://www.viewfinderpanoramas.org/dem3.html.* View Finder Panorama, 2010.

[45] Paraschivoiu, I. *Wind Turbine Design With Emphasis on Darrieus Concept.* Polytechnic International Press - ISBN: 978-2-553-00931-0, 2002.

[46] Park, J.-Y., Lee, S., Sabourin, T., and Park, K. A novel vertical-axis wind turbine for distributed & utility deployment. unpublished.

[47] Peltola, E., Marjaniemi, M., Kaas, J., and Aarnio, E. Heating of wind turbine blades - design and operational experience. *EWEC 97 Proceedings, Dublin, Ireland* (October 1997), 619–621.

[48] Rabah, K., and Osawa, B. *Design and field testing of Savonius wind pump in East Africa.* International Atomic Energy Agency and United Nations Educational Scientific and Cultural Organization - IC-95-60, April 1995.

[49] Rahai, H. R. Development of optimum design configuration and performance for vertical axis wind turbine. Tech. Rep. CEC-500-2005-084, California State University, Long Beach, May 2005.

[50] Rodríguez, M. *Energy supply for an Arctic cottage - Assaqutaq hybrid system.* DTU-Artek, Center for Arktisk Technologi, july 2009.

[51] Saha, U., and Jaya Rajkumar, M. On the performance analysis of savonius rotor with twisted blades. *Energy conversion and Management 31* (2006), 1776–1788.

[52] Savonius, S. The s-rotor and its applications. *Mechanical engineering 53*, 5 (May 1931).

[53] Seifert, H. *Meteorological measurements under icing conditions.* In the BOREAS VI proceedings, Pyh atunturi, Finland, april 2003.

[54] Sheldaht, R., Klimas, P., and L.V.Feltz. Aerodynamic performance of a 5-metre-diameter darrieus turbine with extruded aluminium naca-0015 blades. Tech. Rep. SAND80-0179, Sandia Laboratories, 1980.

[55] T, T. L., and et al, I. B.-G. *State-of-the-art of wind energy in cold climates.* VTT - Working paper 152, 2010.

[56] Tammelin, B., Cavaliere, M., Holttinen, H., Morgan, C., Seifert, H., and Santti, K. *Wind Energy Production in Cold Climate (WECO.* JOR3-CT95-0014, December 1998.

[57] Tammelin, B., Joss, J., Leroy, M., and S antti, K. *Meteorological measurements under icing conditions.* In the BOREAS V, Proceedings, 2001.

[58] Tammelin, B., Kimura, S., S antti, K., and Seifert, H. Icing in europe - effect upon wind power production. *EWEC 99 Proceedings, Nice, France* (March 1999), 1051–1054.

[59] Tammelin, B., Morgan, C., Peltomaa, A., and Hyv onen, R. Ice free anemometers. *EWEC 97 Proceedings of the International Conference, Dublin, Ireland* (October 1997), 389–392.

[60] Tammelin, B., Roos, I., and Hyv onen, R. Wind energy production in cold climate. final report. *ERBIC20CT960001* (1999), 16.

[61] Tammelin, B., and S antti, K. Icing in europe. *BOREAS IV, Hetta, Finland* (April 1998).

[62] Tammelin1, B., and Seifert2, H. *Large wind turbine go into cold climate regions.* EWEC, July 2001.

[63] Testarmata, M. M. Performance and efficiency of a micro hybrid energy system at assaqutaq, greenland. Tech. rep., Technical University of Denmark, Arctic Technologies, 2010.

[64] Vaillant, C. L., Hornok, E., and Varin, M. *Building Renovation in Assaqutaq.* DTU-Artek, Center for Arktisk Technologi, 2009.

[65] VTT. *Expert group study on recommendations for wind energy projects in cold climates.* VTT - Working paper 151, 2009.

[66] VTT Arctic wind. *http://arcticwind.vtt.fi/.* VTT, 2010.

[67] VTT Technical Research Center of Finland. *http://www.vtt.fi/.* VTT, 2010.

[68] Zhang, J. Numerical modeling of vertical axis wind turbine (vawt). Master's thesis, DTU, 2004.

ANNEXES

A.1 Source code for DMI data retrieving

A.1.1 Script shell - data downloading

```
#!/bin/sh
#################################################################
# written by Emmanuel Branlard
#################################################################
for i in 1 2 3 4 5 6 7 8 9 10 11 12; do
        # looping on years
        for j in 2000 2001 2002 2003 2004 2005 2006 2007 2008 2009; do
                # looping on months
                for k in 1 2 3 4 5 6 7 8 9 10 11 12; do
                        wget -E -H -k -K -p `echo "http://www.dmi.dk/
                            dmi/vejrarkiv-gl?region="$i"&year="$j"&
                            month="$k`;
                        #echo '"http://www.dmi.dk/dmi/vejrarkiv-gl?
                            region='$i'&year='$j'&month='$k'"';
                done
        done
done
```

A.1.2 Matlab script - image reading - Main

```
%%%%%%%%%%%%%%%%%%%%%%%%%%%%%%%%%%%%%%%%%%%%%%%%%%%%%%%%%%%%%%%%%%%%%%%%
%%% Main
%%%%%%%%%%%%%%%%%%%%%%%%%%%%%%%%%%%%%%%%%%%%%%%%%%%%%%%%%%%%%%%%%%%%%%%%
clear all;clc;
months=1:12;
years=2000:2009;
loc=[1:9 11 12];
locN={'Qaanaq','Upernavik','Ilulissat','Aasiaat','Sisimiut','
    Kangerlussuaq','Nuuk','Paamiut','Nanortalik','','Tasiilaq','
    Ittoqqortoormiit'};


%%

ds=(3600*24*31)/589;
t=0:ds:(3600*24*31-ds);
d=floor(t/(24*3600));
h=floor((t-d*24*3600)/3600 );
m=floor((t-d*24*3600-h*3600)/60 );
MonthTime=d'*100*100+h'*100+m';


%%
%  loc=[9 11 12];
for iloc=loc
    disp(locN{iloc})
    for iyear=1:length(years)
        year=years(iyear);
        disp(year)
        yearMat=[];
        for imonth=months
            filename=sprintf('servlet/vejrarkiv?parameter=wind&region
                =%d&year=%d&month=%d&country=g',iloc,year,imonth) ;
```

```
31                  M=getXYFromFig(filename,[70 70 70],5,0,0);
32
33                  filename=sprintf('servlet/vejrarkiv?parameter=winddir&
                        region=%d&year=%d&month=%d&country=g',iloc,year,imonth
                        );
34                  Mwinddir=getXYFromFig(filename,[70 70 70],90,0,0);
35
36                  filename=sprintf('servlet/vejrarkiv?parameter=precip&
                        region=%d&year=%d&month=%d&country=g',iloc,year,imonth
                        );
37                  Mprecip=getXYFromFig(filename,[51 73 128],5,0,0);
38
39
40                  %Origin
41                   filename=sprintf('servlet/vejrarkiv?parameter=temp&region
                        =%d&year=%d&month=%d&country=g',iloc,year,imonth);
42                   Mtempr=getXYFromFig(filename,[201 44 41],5,1,0);
43                   Mtempg=getXYFromFig(filename,[89 89 89],5,1,0);
44                   Mtempb=getXYFromFig(filename,[51 73 128],5,1,0);
45
46                  filename=sprintf('servlet/vejrarkiv?parameter=pres&region
                        =%d&year=%d&month=%d&country=g',iloc,year,imonth);
47                  Mpres=getXYFromFig(filename,[70 70 70],10,1,0);
48
49
50
51                  %%% time stamp
52                  M(:,1)=year*100*100*100*100+imonth*100*100*100+MonthTime;
53
54                  %%combining results
55                  MM=[M Mwinddir(:,2) Mprecip(:,2) Mtempr(:,2) Mtempg(:,2)
                        Mtempb(:,2) Mpres(:,2)];
56
57                  %%% taking month length into account
58                   if(imonth==2)
59                        %only 28 days
60                        if(mod(year,4)==0)
61                             MM=MM(1:533,:);
62                        else %only 29 days
63                             MM=MM(1:552,:);
64                        end
65                   end
66                   %only 30 days
67                   if(imonth==4 || imonth==6 || imonth==9 || imonth==11)
68                        MM=MM(1:571,:);
69                   end
70                   %%%storing
71                   yearMat=[yearMat;MM];
72              end
73              filename=sprintf('DMI_wind/%s-%d.csv',locN{iloc},years(iyear))
                    ;
74              %fid=fopen(filename,'w');
75              %fprintf(fid,'Timestamp\tWS(m/s)\tWD(deg)\tPrecip(mm)\tTempMax
                    (deg)\tTempNorm(deg)\tTempMin(deg)\tPressure(hPa)\n');
76              %fclose(fid);
77              dlmwrite(filename,yearMat,'delimiter','\t','precision','%12.2
                    f');
78          end
79      end
```

A.1.3 Sub-function detecting curves

```
function M=getXYFromFig(filename,color,scale,guessLim,doPlot)
%%
% filename='servlet/vejrarkiv?parameter=pres&region=5&year=2009&month=1&country=g';
% doPlot=1;
% guessLim=1;



%%
try
  %warning off;
  [A0, map] = imread(filename);
  %warning on;

if doPlot
    figure(1)
    clf
%     subplot(1,2,1)
    image(A0);
end
%%
if guessLim
   Aymin=A0(306:322,602:638,:);
   Aymax=A0(90:102,602:638,:);
   ymin=readNumber(Aymin);
   ymax=readNumber(Aymax);
end


%% cropping
A0=A0(98:315,11:599,:);
% image(A0)

Acurve=A0*0+255;
Agrid=Acurve;
%%
Y=1:length(A0(:,1,1));
X=1:length(A0(1,:,1));
I=meshgrid(Y,X);
%
rImg=squeeze(A0(:,:,1));
gImg=squeeze(A0(:,:,2));
bImg=squeeze(A0(:,:,3));
rCurve=rImg*0;
rGrid=rCurve;
%%
%extracting curve and grid
bCurve=(rImg==color(1))&(gImg==color(2))&(bImg==color(3));
bGrid=(rImg==196)&(gImg==196)&(bImg==184);

%
rCurve(bCurve)=100;
% Acurve(:,:,1)=rCurve;
% Acurve(:,:,2)=rCurve;
% Acurve(:,:,3)=rCurve;

```

```
57
58  rGrid(bGrid)=100;
59  % Agrid(:,:,1)=rGrid;
60  % Agrid(:,:,2)=rGrid;
61  % Agrid(:,:,3)=rGrid;
62  %% Vertical extent
63  if ~guessLim
64      % Couting grid lines
65      lines=mean(rGrid')/100  >0.5;
66      Ylines=Y(lines);
67      if(length(Ylines)==1)
68          nlines=2;
69      else
70          hgrid=mean(diff(Ylines));
71          nlines=floor(length(Y)/hgrid)+1;
72      end
73      ymin=0;
74      ymax=scale*nlines;
75  end
76  %% Curve data
77  realY=linspace(ymax,ymin,length(Y));
78  xx=linspace(0,31,length(X));
79  yy=X*0+NaN;
80  for i=1:length(X)
81      if(sum(rCurve(:,i)>0)>0)
82          [m ii]=max(rCurve(:,i));
83          yy(i)=realY(ii);
84      end
85  end
86
87  %%
88  %figure
89  %image(Acurve)
90  % image(A0)
91  %%
92
93  if doPlot
94  %   subplot(1,2,2)
95  figure(2)
96      clf
97    plot(xx,yy,'LineWidth',2)
98    ylim([ymin ymax])
99    xlim([0  31])
100   grid on
101   pause(0.5)
102 end
103
104 catch
105   % disp('error');
106     xx=1:589;
107     yy=xx*0+NaN;
108 %   return;
109 end
110
111 M=[xx' yy'];
112   end
```

A.1.4 Sub-function reading numbers

```
function numb=readNumber(A)
%  clear all; clc
%  filename ='servlet/vejrarkiv?parameter=temp&region=3&year=2000&
    month=1&country=g'
%%
%
% A0=imread(filename);
%  image(A0)

%%
% Aymin=A0(306:322,602:638,:);
% Aymin=A0(90:102,602:638,:);
% figure(1)
% clf
% image(A)

rY=squeeze(A(:,:,1));
%%
%
rY(rY~=219)=1;
rY(rY==219)=0;
%%
% figure(2)
% clf
% image(rYmin)
%% detecting characters
I=1:size(rY,1);
I=I(sum(rY')>0);
rstart=min(I);
rend=max(I);

chars=[];
xproj=sum(rY);
j=1;
for i=2:(length(xproj)-1)
    if(xproj(i)>0 && xproj(i-1)==0)
        chars(j).cstart=i;
    end
    if(xproj(i)==0 && xproj(i-1)>0)
        chars(j).cend=i-1;
        chars(j).sum=sum(xproj(chars(j).cstart:(i-1)));
        chars(j).xproj=xproj(chars(j).cstart:(i-1));
        chars(j).length=chars(j).cend-chars(j).cstart+1;
        j=j+1;
    end
end

if(length(chars)==0)
    numb=NaN;
    return;
end
%% detection
numb='';
if(length(chars)>0)
    for j=1:length(chars)
        c=chars(j);
        if(c.length==4)
```

```
57                  if(sum(c.xproj==[1 1 1 1])==4)
58                      numb='-';
59                  end
60                  if(sum(c.xproj==[8 6 6 8])==4)
61                      numb=[numb '0'];
62                  end
63                  if(sum(c.xproj==[5 6 7 6])==4)
64                      numb=[numb '2'];
65                  end
66                  if(sum(c.xproj==[2 3 7 8])==4)
67                      numb=[numb '3'];
68                  end
69                  if(sum(c.xproj==[5 4 5 6])==4)
70                      numb=[numb '5'];
71                  end
72                  if(sum(c.xproj==[8 7 5 6])==4)
73                      numb=[numb '6'];
74                  end
75                  if(sum(c.xproj==[4 6 5 3])==4)
76                      numb=[numb '7'];
77                  end
78                  if(sum(c.xproj==[8 7 7 8])==4)
79                      numb=[numb '8'];
80                  end
81                  if(sum(c.xproj==[6 6 8 8])==4)
82                      numb=[numb '9'];
83                  end
84              end
85              if(c.length==3)
86                  numb=[numb '1'];
87              end
88              if(c.length==5)
89                  numb=[numb '4'];
90              end
91          end
92      end
93      numb=str2num(numb);
94      end
```

A.2 R source code for temperature maps

```
1   setPlottingMethod("png")
2   library(lattice)
3
4   Files=list.files("./",pattern="*.txt")
5   ########################################
6   ### WORLD MEAN TEMPERATURE
7   ########################################
8   worldmean=matrix(0,360,720);
9   for(f in Files){
10          M=read.table(f, sep="\t",header=F)
11          M[M==-999]=NA;
12      worldmean=worldmean+M;
13  }
14  worldmean=worldmean/12;
15
```

```
16
17 titl="World Mean Temperature [deg C] - 1961-1990"
18 beginPlot(titl,showTitle=T)
19         mycontourplot(
20                 t(worldmean),x=seq(-180,180,length.out=ncol(M)),y=seq
                       (-90,90,length.out=nrow(M)),
21         xlab="Longitude [deg]", ylab="Lattitude [deg]",main=titl,
22         nlevel=100)
23 dev.off()
24
25
26
27
28
29 ######################################
30 ### GREENLAND per Seasons
31 ######################################
32 Months=c("January","February","March","April","May","June","July","
       August","September","October","November","December")
33 for(i in 1:length(Files)){
34         M=read.table(Files[i], sep="\t",header=F)
35         long=seq(-180,180,length.out=ncol(M))
36         lat=seq(-90,90,length.out=nrow(M))
37
38         ilong=which(long>-77 & long< -10)
39         ilat=which(lat>59 & lat< 85)
40
41         MM=M[ilat,ilong];
42         MM[MM==-999]=NA;
43
44         titl=paste(Months[i]," -  Mean Temperature [deg C] - 1961-1990
               ",sep="")
45         beginPlot(titl,showTitle=F,width=7,height=6)
46                 mycontourplot(
47                         t(MM),x=long[ilong],y=lat[ilat],
48                 xlab="Longitude [deg]", ylab="Lattitude [deg]",main=""
                       ,
49                 nlevel=100,zlim=c(-43,13))
50         dev.off()
51
52 }
53
54 ######################################
55 ### GREENLAND SASONAL MEAN
56 ######################################
57 titl="Greenland Mean Temperature [deg C] - 1961-1990"
58 beginPlot(titl,showTitle=T)
59         mycontourplot(
60                 t(worldmean[ilat,ilong]),x=long[ilong],y=lat[ilat],
61         xlab="Longitude [deg]", ylab="Lattitude [deg]",main=titl,
62         nlevel=100)
63 dev.off()
```

List of Figures

List of Tables